ISJET

INTERNATIONAL SCIENTIFIC JOURNAL OF ENGINEERING AND TECHNOLOGY

Volume 1 No. 2 July-December 2017

ISSN: 2586-8527

Panyapiwat Institute of Management (PIM)

ISJET

INTERNATIONAL SCIENTIFIC JOURNAL OF ENGINEERING AND TECHNOLOGY

Volume 1 No. 2 July-December 2017

PANYAPIWAT INSTITUTE OF MANAGEMENT

INTERNATIONAL SCIENTIFIC JOURNAL OF ENGINEERING AND TECHNOLOGY (ISJET)
Volume 1 No. 2
July-December 2017

Editorial Staff Contacts
Panyapiwat Institute of Management
85/1 Moo 2, Chaengwattana Rd.,
Bang Talad, Pakkred, Nonthaburi 11120
Tel. 0-2855-1560
https://isjet.pim.ac.th
Email: isjet@pim.ac.th

Contact Printing House
Chulalongkorn University Printing House
Bangkok, Thailand
Tel. 0-2218-3549-50
Fax. 0-2215-3612
http://www.cuprint.chula.ac.th
Email: cuprint@hotmail.com

INTERNATIONAL SCIENTIFIC JOURNAL OF ENGINEERING AND TECHNOLOGY (ISJET)

Volume 1 No. 2 July-December 2017 ISSN 2586-8527

Objective

International Scientific Journal of Engineering and Technology will be dedicated to serving as a forum to share knowledge on research advances in all fields of sciences: Engineering, Technology, Innovation, Information Technology, Management Information System, Logistics and Transportation, Agricultural Science, Animal Science and Aquaculture, Food Science, and other areas in Sciences and Technology. Submissions are welcomed from both PIM as well as other Thai and foreign institutions.

Scope

Engineering, Technology, Innovation, Information Technology, Management Information System, Logistics and Transportation, Agricultural Science, Animal Science and Aquaculture, Food Science, and other areas in Sciences and Technology.

Type of Article

1. Research article
2. Academic article
3. Book review
4. Review article

Reviewing Policy

1. The manuscripts should be approved by at least 2 peer reviewers.
2. The manuscripts should be never published and are not in the approving process of the other periodicals.
3. The content, expression, tables and figures that appearing in the manuscripts have nothing to do with Panyapiwat Institute of Management.
4. Editorial board of International Scientific Journal of Engineering and Technology reserve the right to adjusting and publishing of the manuscripts.

Frequency: 2 issue/year

Every June and December
The first issue: January-June
The second issue: July-December

INTERNATIONAL SCIENTIFIC JOURNAL OF ENGINEERING AND TECHNOLOGY (ISJET)

Volume 1 No. 2 July-December 2017

ISSN 2586-8527

Peer Reviewers

Assoc. Prof. Dr. Parinya Sanguansat	Panyapiwat Institute of Management
Assoc. Prof. Dr. Paritud Bhadhubanyong	Panyapiwat Institute of Management
Assoc. Prof. Dr. Pongsatorn Sedtheetorn	Mahidol University
Assoc. Prof. Dr. Suksan Prombanpong	King Mongkut's University of Technology Thonburi
Asst. Prof. Dr. Chutisant Kerdvibulvech	National Institute of Development Administration (NIDA)
Asst. Prof. Dr. Nivet Chirawichitchai	Sripatum University
Asst. Prof. Dr. Paitoon Sirioran	Panyapiwat Institute of Management
Asst. Prof. Dr. Weerawut Thanhikam	Panyapiwat Institute of Management
Dr. Sujin Wanchat	Kasetsart University, Sriracha Campus
Dr. Tantikorn Pichpibul	Panyapiwat Institute of Management

INTERNATIONAL SCIENTIFIC JOURNAL OF ENGINEERING AND TECHNOLOGY (ISJET)
Panyapiwat Institute of Management
85/1 Moo 2, Chaengwattana Rd.,
Bang Talad, Pakkred, Nonthaburi 11120,
Thailand

Dear colleagues,

We are pleased to invite you to submit research article, academic article, review article, or book review for the INTERNATIONAL SCIENTIFIC JOURNAL OF ENGINEERING AND TECHNOLOGY (ISJET). This journal will be dedicated to serving as a forum to share knowledge on research advances in all fields of sciences: Engineering, Technology, Innovation, Information Technology, Management Information System, Logistics and Transportation, Agricultural Science, Animal Science and Aquaculture, Food Science, and other areas in Sciences and Technology. Submissions are welcomed from both Thai and foreign institutions.

Submitted manuscripts should not have been published previously, nor be under consideration for publication elsewhere. All manuscripts are refereed through a peer-review process. If you are interested in joining us, please submitted manuscripts via editor in chief E-mail at parinyasan@pim.ac.th. Please read our template and instructions for authors that attached to the E-mail before submitting.

With kind regards,

Assoc. Prof. Dr. Parinya Sanguansat
Editor in Chief

Contact:
Miss Suchinda Chaluai
Tel. 0-2855-1560
E-mail: suchindacha@pim.ac.th

CONTENTS

- **Application of Reverse Engineering and Additive Manufacturing for Prosthesis Fabrication Process Improvement** 1
  Sathani Plotthao, Pornsuda Phonsa-ard, Thittikorn Phattanaphibul and Thongchai Chinkatham

- **Improving Capability in Small Thai Manufacturing Companies** 6
  John T. H. Pearce and Paritud Bhandhubanyong

- **Influence of Fiber Length of the Fractionated Pulp and its Fiber Swelling Capacity on Compressive Resistance and Other Strength Properties of Corrugating Medium Handsheet** 14
  Wiroj Savangsrisutikun and Phichit Somboon

- **Investigation of Copper Anode Treatment** 19
  Jarunee Kraikaew and Brajendra Mishra

- **Modeling the Dynamic Individual Activity Decision Behavior Through the Influence Diagram Model** 30
  Natachai Wongchavalidkul

- **Neural Network Modeling for Predicting Electric Power Generation From Sea Waves** 38
  Pisit Phokharatkul, Visarut Ahkuputra, Chom Kimpan and Ekkarit Maneenoi


PIM
PANYAPIWAT
INSTITUTE OF MANAGEMENT
สถาบันการจัดการปัญญาภิวัฒน์

Application of Reverse Engineering and Additive Manufacturing for Prosthesis Fabrication Process Improvement

Sathani Plotthao, Pornsuda Phonsa-ard, Thittikorn Phattanaphibul* and Thongchai Chinkatham

Integrated Design and Manufacturing Systems Research Unit,
Faculty of Engineering at Sriracha, Kasetsart University, Sriracha Campus, Chonburi, Thailand
E-mail: thittikorn@eng.src.ku.ac.th*

***Abstract*—Reverse engineering (RE) as well as Additive manufacturing (AM) are two potential technologies that have been widely used in product development. Presented in this paper is to apply both technologies to improve prosthesis fabrication that is typically skill intensive process. A case study of abelow-knee amputee was presented. Rather than making the positive mold of the stump by trial and error, a handheld 3D scanner was used to collect the shape of the amputee's stump. The obtained point cloud data were reconstructed to be the surface model for making the positive mold by an FDM-based additive manufacturing machine. By using this approach, the socket of the prosthesis could fit with the amputee's stump effectively but the fabrication time and cost were still issues to be further improved.**

***Index Terms*—Prosthesis, Amputation, Reverse engineering, RE, Additive manufacturing, AM.**

I. Introduction

Reverse engineering (RE) is a digital technology that brings a physical object directly to a 3D-CAD model. By using scanning or measuring devices, the surface data of the object, often called point cloud data, are captured and then enhanced via RE software to create the 3D-CAD model. Up to date, this technology has been widely used in several applications including medical area [1]. Computer tomography scanning (CT-scan) and magnetic resonance imaging (MRI) are two well-known devices using in this area. Detailed images of internal organs, e.g., brain, heart, bones, soft tissue and blood vessels, are generated by X-rays (for CT-scan) and magnetic fields (for MRI). These image sallow the doctor be able to see the inside of the human body for diagnosis.

A fabrication process of prosthesis, an artificial device used for replacement of the missing limb, is another application that RE has been recognized as a potential technology to help the madeprosthesis-effectively fit with the amputee [2-4]. Typically the prosthesis consists of several standard parts that are used based on weight and height of the amputee except prosthesis's socket that must be customized for everyone to achieve successful rehabilitation. Fig. I shows an example of lower prosthesis.

According to the report of National Statistical Office (NSO) of Thailand, there were about 46,000 lower amputations in 2006. Furthermore the report indicated that approximately 3,500 amputations occur each year. Two majorities of these cases were (1) disease causing from peripheral artery disease or PAD (e.g. diabetes) and (2) traffic accidents. Astoundingly, almost 20,000 amputees had less opportunity to access appropriate prosthesis due to several constraints, for example, cost and lead time. Time for fabrication process of the donated prosthesis is an issue to be addressed in this study. Usually the prosthesis is made manually by the prosthetic technician. The fabrication's lead time is two days on average and varied dependent on skills of the technician and complexity of the prosthesis that must be fitted with the stump of the amputee.

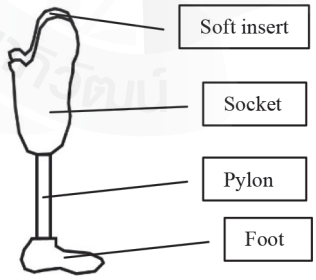

Fig. I. Main components of lower prosthesis.

Presented in this paper is an attempt to apply RE to help improve the prosthesis fabrication process. In addition, additive manufacturing (AM), another technology always used in parallel with RE, is also applied. RE and AM have been applied to shorten the fabrication time and to reduce the error of the created positive mold of the stump that is then used for creating the prosthesis socket. Abelow- knee (BK) prosthesis was considered as a case study. In the next

section, the current fabrication process is introduced. Then the materials and methods are presented in the section III. Results and discussions are provided in the section IV. Conclusions and recommendations are addressed at the last section.

II. Current Prosthesis Fabrication Process

Sand casting technique according to the Center for International Rehabilitation (CIR) [5], Chicago, USA, often called CIR sand casting, is a prosthesis fabrication technique widely used nowadays. This technique includes four main steps: (1) amputee's stump preparation, (2) negative mold fabrication, (3) positive mold fabrication, and (4) soft insert and socket fabrication. In this study, CIR sand casting technique was applied to the case study amputee as benchmark. The detail is given as the followings.

Firstly, the stump should be prepared in suitable conditions [6]. The incision should be neat and the wound should be fully recovered. Besides, the leg should have sufficient length and strong muscles. After initial checking as aforementioned, the stump is covered with a thin cling filmin order to make the stump fits firmly. Foam or cotton paddings are applied to all bony prominences and pressure sensitive areas for pressure relief. Then dimensions of the stump are measured for reference including antero-posterior, mediolateral diameter and length of the stump. The stump is then covered with three layers of elastic stockinette/plastic bag/elastic stockinette.

After preparation step, the stump is inserted into a casting bag filled with polystyrene (PS) beads. In addition, the rim of the bag should be above the knee. Vacuum pressure is applied to the casting bag until the PS beads become the solid negative mold of the stump.

The positive mold of the stump is fabricated by replacing the stump with sand. After removing the stump, a vacuum mandrel is inserted into the center of the negative mold that is subsequently filled with sand to the brim. The vacuum pressure is applied to the plastic bag to form the positive mold. The dimensions of formed mold must be checked for comfortable fit between the stump and socket. Thus minor modifications may be done by pushing the positive mold with thumb or smooth pipe.

Finally, the modified positive mold is used for creating the soft insert and socket. The soft insert is made from a pelite liner via drape vacuum forming. Similarly, the soft insert is used as another mold for making the socket via drape vacuum forming. A thermoplastic sheetis applied for more durable usage. The fabricated socket is then assembled with modular pylon, foot, and shoe.

III. Materials and Method

According to the prosthetic principles, the socket must be fabricated in the correct way to ensure the prosthesis control. Each movement between the amputee's stump and socket may result in unsafe conditions and pain while walking and postures [2]. The current prosthesis fabrication process is mostly hand-made that human error may occur and also time consuming. In this study, RE was used to directly acquire the morphology of the amputee's stump instead of the created negative mold. Then AM was used to fabricate the positive mold from the acquired data. By this combination, the socket will be fabricated with high accuracy resulted in high degree of comfortability

A. Stump Morphology Acquisition

Structured light system is another non-contact technique to acquire surface data of the object like CT-scan and MRI. A known pattern light is projected onto the target and the occurred deformed pattern is then captured by a camera or other image detection devices [7].

To acquire morphology of the stump, ahandheld structured light 3D scanner (Artec Eva Lite) was used. Its resolution and point accuracy were 0.5 mm and 0.1 mm respectively. After stump preparation step as mentioned, the stump was scanned to acquire the point cloud data. The obtained data were checked and edited by using Artec Studio 10 (Professional Version) software.

B. Stump Positive Mold Fabrication

Fused deposition modelling (FDM) is a well-known commercial AM technique. A physical model is manufactured by deposition of the fused thermoplastic filament, e.g., Poly-lactic acid (PLA) and Acrylonitrile butadiene styrene (ABS).

The edited point cloud data were inputted to an RE software for generating a surface model. Then it was converted to be a shell-like model before uploading to FDM machine (Stratasys Dimension Elite). The stump positive mold was fabricated with ABS filament (∅1.75 mm).

IV. Results and Discussions

A case study was a 60 years old Thai male who had below-knee (transtibial) amputation on the right leg. His stump could passall criteria for making prosthesis. Then the stump was prepared as the followings: (1) covered with cling film, (2) applied foam paddings at bony prominences and pressure sensitive areas, (3) measured dimensions of stump, and (4) covered with elastic stockinette.

While scanning the stump, the amputee should be in standing posture in order to avoid unwanted components. Multiple scans might be performed to obtain all data. All point cloud data were combined in Artec Studio 10 software by using pair matches between the same points on different scans. The complete point cloud data should be checked for its dimensions accuracy by comparing to the measured

dimensions of the stump. Fig. II (a)-(d) presents the stump morphology acquisition via 3D scanner.

The complete point cloud data were converted to surface model with thickness of 3 mm by using the RE software. Subsequently, the process parameters and part's orientation, including support structure, were set by using CatalystEX 4.5 software. Layer thickness was at 0.254 mm. Fig. III (b) presents the part's orientation and support structure. According to this setup, the approximate fabrication time was 28.49 hrs. Fig. III (d) shows the finish fabricated part.

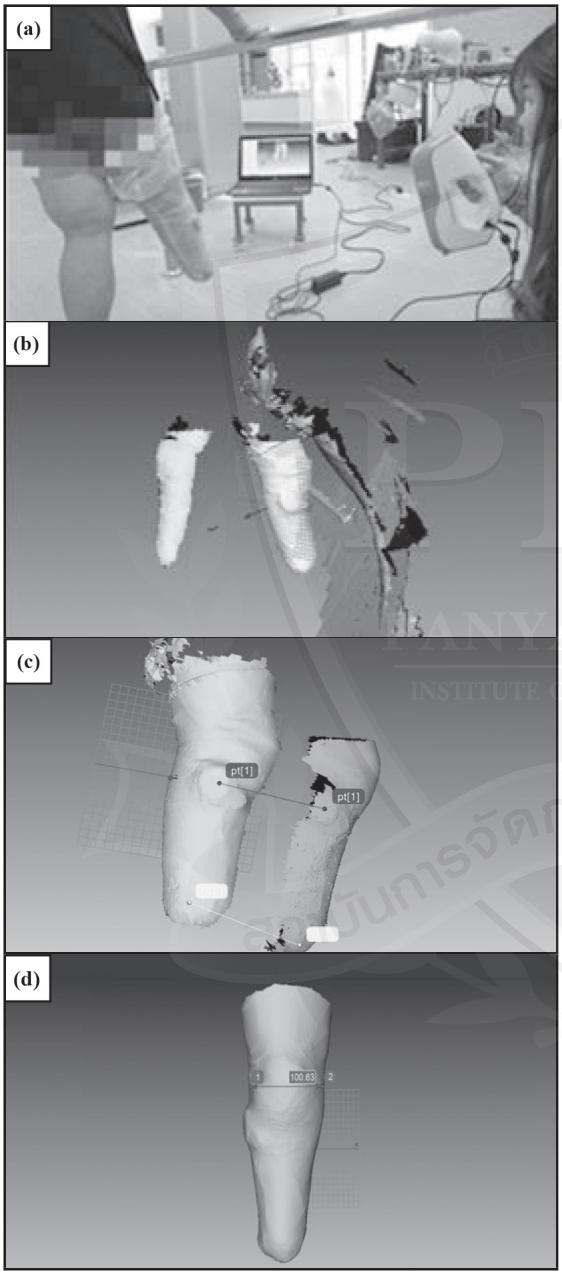

Fig. II. Stump morphology acquisition: (a) scanning the stump, (b) point cloud data before being combined, (c) pair matches between the points, (d) complete point cloud data.

Similar to the positive mold made by CIR sand casting, the printed positive mold was modified to achieve comfortable fit. Then the modified mold was used for fabricating the soft insert and socket respectively. The fabrication processes were drape vacuum forming as mentioned in the section II. Fig. IV (a) shows the fabricated soft insert and socket. After loading test, the amputee felt comfortable fit and no pain while applying load as shown in Fig. IV (b). Result illustrated the potential promise to lower the risk of discomfort problem unlike the current approach that the fabricated soft insert and socket were often modified. Sometimes the process must be repeated due to severe discomf

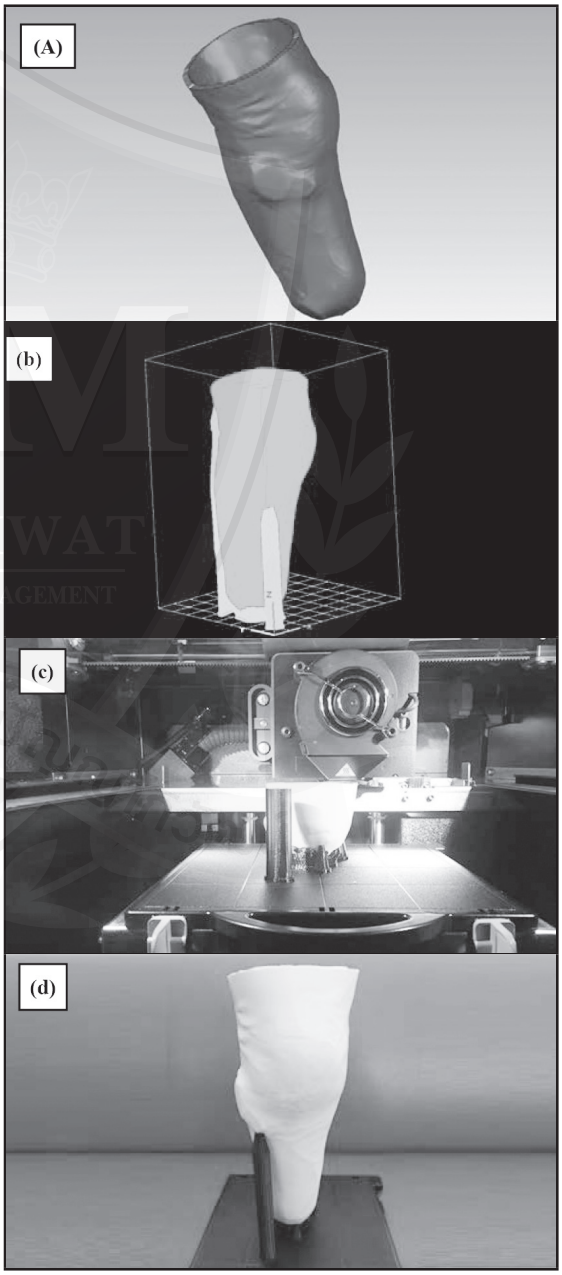

Fig. III. Stump positive mold fabrication: (a) surface model with thickness of 3 mm, (b) part's orientation and support structure, (c) part in FDM machine, (d) finish fabricated part.

However, the total fabrication time was unclear-whether it could be considered as success. For ideal case that the amputee felt comfortable fit in the first time, the current fabrication process spent 2.92 hrs. while the presented approach spent 31.04 hrs. In practice, the fit's quality was depended on skill and experience of the technician. Therefore, the current fabrication process may use more time. Besides, the cost will be higher due to the replication of the process. Table I presents the time used in the current and presented fabrication approach.

In term of cost, the fabricated positive mold of the experimental approach (ABS model) was more expensive than the current approach (Sand model). The cost of ABS model was 15,000 Baht according to the volume of material while the other one was only 550 Baht. However, the durability of the ABS model shows an outstanding benefit over the sand model that might be deformed while fabricating the soft insert and socket.

TABLE I
COMPARISON OF FABRICATION TIME

Step	Fabrication approach	
	Current	RE + AM
1	0.17 hrs	0.17 hrs
2	0.08 hrs (Negative PS mold)	0.05 hrs (Stump scanning)
3	0.17 hrs (Positive sand mold) 0.50 hrs (Modification)	0.33 hrs (Point cloud & surface model) 28.49 hrs (3D printing)
4	2.00 hrs 2.92 hrs	2.00 hrs 31.04 hrs

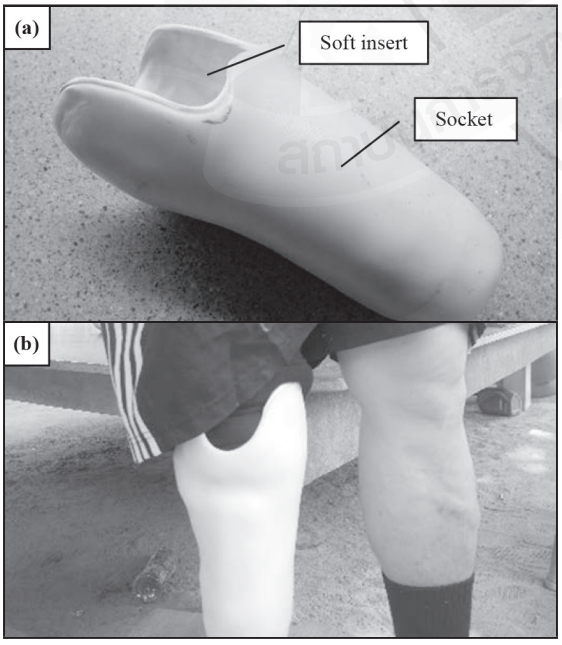

Fig. IV. The fabricated soft insert and socket: (a) before test, (b) during test.

With the results from this case study, RE and AM technologies presented a potential promise for Thai prosthesis fabrication sector. Although this combination was not a new technology and also quite expensive process, it was still an interesting technology comparing to others, e.g., power knee and power foot [8], since the prosthesis could be custom-made for each amputee. In order for this approach to be realized in Thailand especially in rural area, the instrumentand fabrication costs should be subsidized by government. Besides, further studies on lowering both fabrication time and cost were still required. Process parameters of AM were tended to be adjusted to increase the fabrication speed and new part material might be considered to encourage the price of prosthesis be more affordable [9].

V. Conclusion and Recommendations

In this study, reverse engineering (RE) and additive manufacturing (AM) were applied to improve the below-knee prosthesis fabrication process. Morphology of the amputee's stump is an important factor affecting degree of comfortability while the prosthesis being used. RE, a potential technology to extract the knowledge and design from any physical object, is used for this purpose. To convert the obtained data to the real object, AM was applied. By using this approach, the prosthesis could be made and duplicated with high accuracy unlike the current approach that was skill intensive process. However, the total fabrication time and also cost were still required further improvement. Adjusting the process parameters and finding new part material of AM might be considered to achieve both issues.

Acknowledgment

The authors would like to express sincere thanks to the case study amputee as well as the royal leg factory, Phanomsarakham hospital, Chachoengsao, for their collaboration.

References

[1] M. Sokovic, and J. Kopac, "RE (reverse engineering) as necessary phase by rapid product development," *J. Mater. Process. Technol.*, vol. 175, no. 1, pp. 398-403. 2006.

[2] G. Colombo, S. Filippi, C. Rizzi, and F. Rotini, "A new design paradigm for the development of custom-fit soft sockets for lower limb prostheses," *Comput. Ind.*, vol. 61, no. 6, pp. 513-523. Aug. 2010.

[3] Z. Shuxian, Z. Wanhua, and L. Bingheng, "3D reconstruction of the structure of a residual limb for customising the design of a prosthetic socket," *Med. Eng. Phys.*, vol. 27, no. 1, pp. 67-74. Jan. 2005.

[4] WC. Lee, and M. Zhang, "Using computational simulation to aid in the prediction of socket fit: A preliminary study," *Med. Eng. Phys.*, vol. 29, no. 8, pp. 923-929. Oct. 2007.

[5] Y. Wu, H. Casanova, WK. Smith, M. Edwards, and DS. Childress, "CIR sand casting system for trans-tibial socket," *Prosthet. Orthot. Int.*, vol. 27, no. 2, pp. 146-152. Aug. 2003.

[6] Prostheses Foundation of H.R.H the Princess Mother,"Things to know before fitting the prosthesis," Available: http://www.prosthesesfoundation.or.th/en/knowledge/301

[7] S. Rianmora, and P. Koomsap, "Structured light system-based selective data acquisition," *Robot. Comput. Integr. Manuf.*, vol. 27, no. 4, pp. 870-880. Aug. 2011.
[8] J. Z. Laferrier, and R. Gailey, "Advances in lower-limb prosthetic technology," *Phys. Med. Rehabil. Clin. N. Am.*, vol. 21, no. 1, pp. 87-110. Feb. 2010.
[9] J. Andrysek, "Lower-limb prosthetic technologies in the developing world: a review of literature from 1994-2010," *Prosthet. Orthot. Int.*, vol. 34, no.4, pp. 378-398. 2010.

Sathani Plotthao received her B. Eng. in Industrial and Systems Engineering from Kasetsart University, Sriracha Campus.

Pornsuda Phonsa ard received her B. Eng. in Industrial and Systems Engineering from Kasetsart University, Sriracha Campus.

Thittikorn Phattanaphibul is an assistant professor in Integrated Design and Manufacturing Systems (IDMS) Research Unit, Faculty of Engineering at Sriracha, Kasetsart University, Sriracha Campus.

He received his D. Eng. in Industrial and Manufacturing Engineering from Asian Institute of Technology, Thailand. His research interests are Additive Manufacturing, Design & Development of Automation System, and Automotive Mold & Die design.

Thongchai Chinkatham is a lecturer and researcher in Integrated Design and Manufacturing Systems (IDMS) Research Unit, Faculty of Engineering at Sriracha, Kasetsart University, Sriracha Campus.

He received his Ph.D. in Industrial Engineering/Design from University of Strasbourg, France. His research interests are Technical System Design Engineering, Innovation Pipeline Management, Intellectual Property, and Robotic & Automation.

Improving Capability in Small Thai Manufacturing Companies

John T. H. Pearce and Paritud Bhandhubanyong

Department of Automotive Manufacturing Engineering, Panyapiwat Institute of Management, Nonthaburi, Thailand
E-mail: jthp70@gmail.com, paritudbha@pim.ac.th

***Abstract*— Statistical Process Control (SPC) is definitely one of the most powerful scientific methods for process control in manufacturing industry. Application of suitable SPC tools and techniques, e.g., graphical representation, scatter diagrams, variable and attribute control chartsand the assessment ofcapability via suitable indices could help improve and assure product quality and minimize losses due to non-conformity. Application of machine and process capability studies would be really beneficial for small and medium sized manufacturers. Capability assessment involves relatively little cost and effort but can contribute to significant improvement in performance. This paper reviews and explains the background to the application of machine and process capability studies in manufacturing processes. Capability study is also shown to be very useful in the development of a new process or product as well as for ongoing production.**

***Index Terms*—Statistical Process Control, Machine Capability Study, Process Capability Study**

I. Introduction

Capability is the power or ability to do something. In reviewing the competitiveness of Thai industries, especially in the automotive sector, a number of recent studies [1-3] have considered approaches in policy and strategy that may be used towards improving capabilities in Research & Development and Innovation in parts producers. This paper considers the situation in small Thai manufacturing companies but, rather than discuss policy for capability improvements, it outlines some practical steps that can be taken by such small companies to improve their technical performance. By using basic statistical techniques improvements in ability to satisfy customer requirements which can be made with minimum investment apart from time and effort.

Much of the manufacturing industry in Thailand is associated with the automotive sector. Hence, in discussing capability and its improvement, reference is made to the special requirements of this sector. Many small companies provide material or components to OEM automotive parts suppliers or themselves produce replacement parts. It is therefore important that such small manufacturers have some understanding of the requirements of the automotive sector regarding quality systems and in particular the application of capability studies as part of Statistical Process Control (SPC) in general.

One Thai company that applies statistical process parameters such as Cp and Cpk found that by monitoring these two parameters the quality of outgoing products could be quantified before dispatch to customers. Hence quality assurance targets could be satisfied thus minimizing product recall and its associated penalties while maintaining customer confidence.

II. Variation in Processes

A given process or machine cannot produce consecutive items which are identical in every respect. SPC techniques via the application of variable and attribute control charts recognize variation in processes and divide the sources of such variation into two types called *Common* and *Special* causes [4]. Common causes occur randomly and are always present during the operation of a process, for example, slight variations within compositional specifications, temperature differences between first and last castings poured out of a ladle, limitations of temperature control in heat treatment furnaces, acceptable tool wear in machining, vibration in machines, etc. Common causes result in variation which is the characteristic of the process and which is *predictable within set limits*. In contrast Special causes are not inherent in a process and give rise to *variation which is not predictable*. Examples of special causes include use of incorrect raw materials, temperature controller not working correctly, heating or cooling rates in heat treatment incorrect, work by incorrectly or insufficiently trained operators, etc.

During the introduction of SPC into a company, special cause variations in processes are identified and eliminated such that only common cause variations remain, resulting in processes which are predictable. Predictable processes, free from special cause variation, are said to be in a *"state of statistical control"*.

Common cause variation may then be examined and be gradually reduced leading to more consistent processes and products. The level of common cause variation can be compared with component tolerances and property requirements to assess both *Machine* and *Process Capability*. Such capability studies determine whether the customer design requirements and tolerances can be satisfied in a predictable manner over an extended run of production.

Variation from a machine or process usually follows a certain pattern. The simplest way of showing this pattern, i.e. the distribution of the results, is to arrange the measured values or data in the form of a bar chart or histogram. If a large number of measurements are taken and the accuracy of measurement is high, the bars on the bar chart would be narrow and a smooth curve could be drawn to model the distribution as shown in Fig. I. In most cases variation usually follows a bell shape called a *Normal Distribution*. Other types of distribution can also occur e.g. *Skew distributions*.

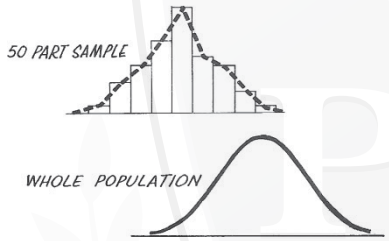

Fig. I. Distribution in a 50 part sample and the whole population [5].

Distributions may differ in setting, in variation and in shape as shown in Fig. II.

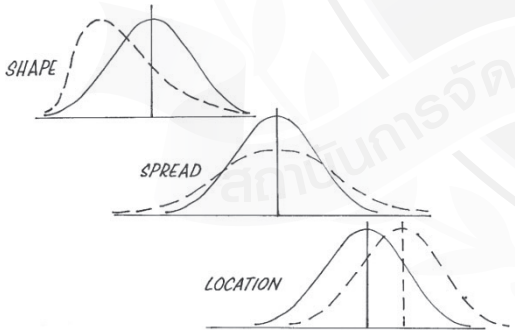

Fig. II. The shape, spread (variation) and location (setting) of distributions [5].

Mathematical models of distributions enable confident predictions to be made about process variables and/or product characteristics. A normal distribution is described by the *Mean (or average) value, X bar* and by *its Standard Deviation, s or σ (sigma)*. The mean (X bar) is a measure of the central value of a normal distribution and describes the setting or location of a process or product characteristic. Standard deviation (s) is a measure of variation or spread in a process or product characteristic. It can be calculated from a standard formula or found by simple graphical methods as in a machine capability study. The use of standard deviation to describe spread about the mean value is shown in Figure III, which illustrates the % spread of results between +1, +2, +3 and +4 standard deviations about X bar. For example if the mean and standard deviation of a set of measurements are 100 and 1 respectively, then we expect 68.26% of the values to lie between 99 and 101, 95.46% between 98 and 102, 99.73% between 97 and 103, and 99.994% between 96 and 104. If process characteristics do not alter, then these predictions should remain true for all subsequent runs of production. These values can be used to assess the capability of a process against customer requirements. This is the basis of :

• Short term *Machine Capability* studies, which are carried out to establish the capability of a machine or process to satisfy the required specification or tolerances *prior to an extended run of production.*

• Longer term *Process Capability* studies which are on-going and *performed during runs of production* using data obtained via plotting of variable SPC control charts.

III. Machine Capability Studies

A machine capability study provides a snap-shot of the process to determine if the process is capable in the short term of meeting customer requirements and tolerances before the start of production. Such studies first became more widely used in parts manufacture when they were made mandatory in the SPC Instruction Guide issued by the Ford Motor Company in 1984 as part of the company's Quality System Standard Q-101 [5]. Each machine capability study is short term and is based on a prenominated sample size of statistically acceptable proportions, this is normally 50 parts. The sample batch is taken as part of a normal production run after any "start-up" or "warm up" fluctuations have been removed. The process parameters must not be altered during the sample run. The required measurements of dimensions, weight, strength, etc. are then performed on each of the 50 parts which have been consecutively produced. The measured values are entered onto a machine capability study sheet as in the example shown in Fig. III.

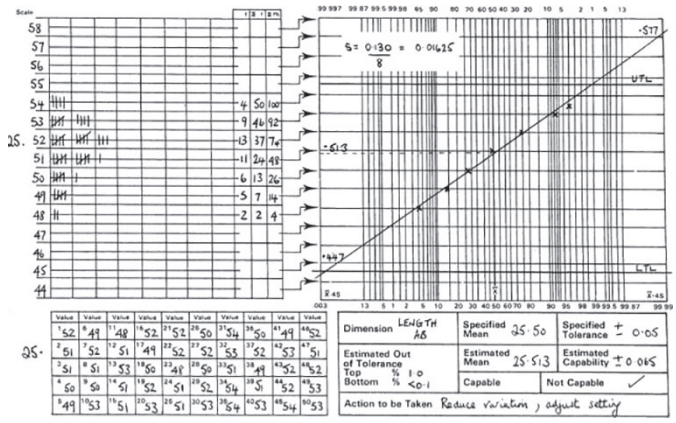

Fig. III. Example of a machine capability study.

The requirement for the part dimension AB is 25.50 +/- 0.05mm. The 50 measured values are entered onto the study sheet and then used to draw up a tally chart which indicates the shape of the distribution. For ease of reading only the figures after the decimal point are given. The tally values are converted to % values and each value plotted on the probability paper at each upper class limit using the "step-up" arrows. The study shows that variation must be reduced and the setting adjusted.

In this sheet, probability paper is used to present a normal distribution as a straight line to enable the results to be extrapolated to +4s and –4s values. This example shows that for the key dimension AB the process is providing a mean value of 25.513 with a 4s variation of 0.065. The customer requires a mean of 25.5 with a 4s variation less than 0.05. Hence the current production set up is not capable of meeting the needs of the customer; so the producer must adjust the process to reduce variation and to reset the process mean to the target of 25.5.

The standard deviation s (σ) is estimated from the slope of the capability study plot on the probability paper. Using this value of s the result of a machine capability study may be summarized by two index values called Cm and Cmk.

Spread is assessed by the machine capability index Cm which is given by(1):

$$Cm = \frac{(USL-LSL)}{6s} \quad (1)$$

Where USL is the Upper specification limit, USL is the Lower specification limit (LSL) and s is the estimated standard deviation.

Using s and the mean value X bar the setting and spread are assessed by the index Cmk which is given by the minimum of the two values calculated from (2) and (3) :

$$Cmk1 = \frac{USL-X\ bar}{3s} \quad (2)$$

$$Cmk2 = \frac{Xbar-LSL}{3s} \quad (3)$$

When the process is set at the specified mean, the two calculated values for Cmk will be the same and will equal Cm. When the process is not on target, the two values for Cmk will be different and the lowest value is reported. In satisfying the original motor industry requirements the minimum requirement for both Cm and Cmk is a value of 1.33 i.e. when the mean value (setting) is on target the variation of +/-4s must not be greater than the specified tolerance (USL - LSL). For a situation where capability is just satisfied, then 8 (+/-4) standard deviations equals the total specified tolerance. When Cm and Cmk both equal 1.33 then 99.994% of production is expected to be within specification. A Cm value smaller than 1.33 shows that the variation is too large and specified tolerances cannot be satisfied i.e. the process is not capable. This is illustrated by the example in Fig. III for which the calculated Cm value is 1.03, with Cmk values of 1.29 and 0.76. The lower value of 0.76 is quoted.

The automotive industry continues to tighten quality assurance standards for parts suppliers. Towards reduced variation, depending on the complexity of the part and the manufacturing method, a minimum short term capability index of 1.67 is required.

Machine capability is an approximate measure of potential capability when a process or a machine is being commissioned at the start of a new product or after a break in production. For example, in high pressure die casting (HPDC) where a new die set is brought into production for the first time or a previously used die set is re-fitted to the HPDC machine for further production runs. Machine capability studies are therefore useful in providing an audit of a process. But it is very important to note that, quite often machine capability data is obtained without sufficient data being available to determine whether or not the process in question is in a state of statistical control. Hence although machine capability measurements contribute to correctly starting up production, they cannot be used for long term predictions of process performance. For the longer term capability must be assessed over

an extended period of time via Process Capability studies *after all special cause variations have been removed.* The process is then in a state of statistical control and therefore predictable. The changing situation with time towards achieving a stable process is illustrated by Fig. IV.

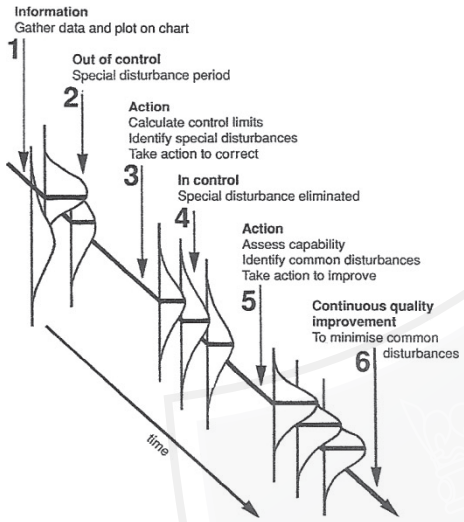

Fig. IV. Stages in process improvement [14] Process Capability is assessed at Step 5 after all special cause variation is removed and the process in a state of statistical control

When the Q-101 Standard was revised to become part of Quality System Requirements QS-9000 in 1994 [6], the approach to capability was modified and Capability was re-defined as *"the total range of inherent variation in a stable process".* As a consequence, as outlined in the section below on process capability, new descriptions were given to the type of capability index to be reported.

For small manufacturing companies, who are not seeking to achieve compliance with QS-9000 or other automotive standards, the application of machine capability studies via probability paper plotting remains a useful practical tool when setting up their processes. When judging initial performance, it is not always necessary to take measurements on 50 parts. Using a cumulative percentage plot for individual values, an estimate of likely variation can be obtained from as few as 15 measurements. This is often called a "pass-off" capability plot; an example of this method is given in Fig. V.

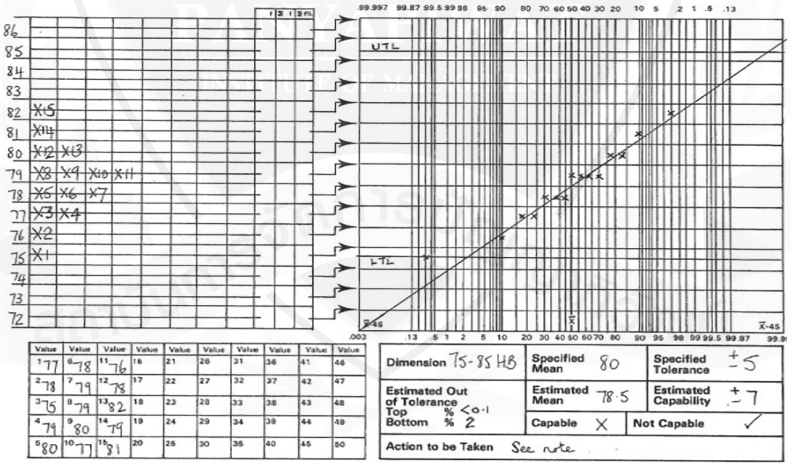

Fig. V. Example of a "Pass-Off" study using only 15 measurements.

A company is starting production of a new casting design in a Al-Mg-5Si alloy using gravity diecasting (permanent mould) and needs to satisfy a specification for Brinell hardness after precipitation heat treatment of 80 +/- 5 HB. To asses initial performance the hardness at a fixed position is measured for each of the first trial batch of 15 castings. Instead of using a tally chart each individual result is plotted in order of magnitude from 1 to 15 as indicated.

Plotting positions are calculated for each result in order of magnitude at a cumulative % value (p) given by (4):

$$p = \frac{\left(i-\frac{1}{2}\right)x100}{n} \tag{4}$$

For value no. 1 p = 3%, for no.2 p = 10%, and so on to for no 15, p= 97%. Each cumulative % value is plotted at the measured value; the "step- up" arrows are not used for individualvalues. Where there is more than one measurement of a particular value the calculated % values are plotted side by side at the same measurement as shown. Plotting of the values in this way indicates the shape of the variation as for a tally chart. In this example the estimated capability is +/- 7 with the mean value below target predicting that unless process control is improved about 2% of production will have too low a hardness. Hence the company must look at tighter control of variables such as composition, pouring temperature, die pre-heat, cooling time, and heat treatment conditions such as ageing time andtemperature towards satisfying the customer requirements.

IV. Process Capability Studies

When using variable control charts, spread is assessed simply by determining the Range R of a small number of measurements taken on consecutively produced parts or parts taken from the same batch of production; in the latter case, for example, this may be parts taken from suitable positions within a tray of heat treated material. In conventional Mean (X bar) and Range (R) charts, the range is the difference between the largest and smallest value in a group of measurements (e.g. dimensions or hardness values of 4 or 5 items). Alternatively where only single measurements can be used (e.g. carbon equivalent liquidus determination, or measurement of liquid metal temperature in a pouring ladle), difference between consecutive values are expressed as a moving- range when using Reading (X) – Moving Range charts [7].

When control charting has shown that all special causes have been eliminated and that only common cause variation exists (at position 5 in Fig. IV), then standard deviation s is estimated from the mean range values using statistical constants and process capability described by calculating the indexes Cp and Cpk as for machine capability. As for Cmk, when the process is not centered on the target value Cpk will have two different values and the lower value is reported.

Cp and Cpk can be calculated by (5) and (6);

$$p = \frac{\left(i-\frac{1}{2}\right)x100}{n} \quad (5)$$

In (5), (6) and (7) USL and LSL are respectively the upper and lower specification limits and s is the estimated standard deviation.

Cpk is given by the minimum of the two values CPU from (6) or CPL from (7):

$$Cp = \frac{USL-LSL}{6s} \quad (6)$$

$$CPU = \frac{USL-X\ double\ bar}{3s} \quad (7)$$

CPU is a measure of setting X double bar (the overall process mean) in relation to the upper specification limit USL, while CPL compares this mean value with the lower specification limit.

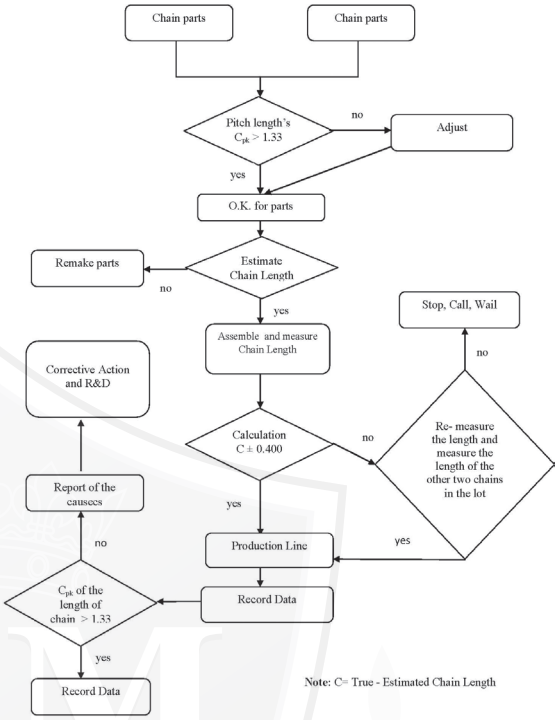

Fig. VI. Flow process of Cpk application in a Thai roller chain manufacturing company

Fig. VI. shows the quality control process of the length of the roller chain in a Thai company before and after assembly. The dimension of each part has been measured and Cpk of the pitch length would be calculated. When the parts are ready, the chain length would be estimated and the partsproceed to assembly. Parameter C which is the difference between the measured chain length and the estimated value would be determined. Actual production would be started then or after any required corrective actions were taken. It was found that the proportion of length defectives in final products was reduced from 0.14% to zero after the Cpkapproach was applied to the process.

In the original auto-industry requirements the minimum required value for both Cp and Cpk is 1.0 i.e. over the long term, when the setting is on target, at least 99.73% of production should be within specification [4, 5]. As for short term capability suppliers are required to continually reduce variation with minimum process capability requirements being increased to 1,33.

When QS-9000 was issued, as part of the Production Part Approval Process (PPAP), requirements for potential suppliers, emphasis was placed on Preliminary Process Capability studies rather than on Machine Capability. Attention was also given to the question

of accuracy and reliability of any measurements used in assessing variation and the automotive industry guidelines for Measurement Systems Analysis were revised [8]. If measuring gauges or any other pieces of testing equipment are not correctly calibrated and kept well-maintained, then we cannot have confidence in the resultant measured data and such data will be misleading in studying the capability of machines or processes. In small companies seeking to improve their performance the purchase, calibration and maintenance of measuring and test devices and training in correct usage is the main area where investment is needed.

Preliminary Process Capability studies are normally carried out at key stages in the development of a new process or product. In a Preliminary Process study, the data is required to be collected and analyzed using X bar and R charting. In reporting capability at least 25 sub-groups of data with at least 100 individual readings must be used. As for Cp and Cpk studies the overall processes mean (X double bar) is taken as a measure of setting with respect to the target value. Estimated standard deviation s (variation) are determined via the initial control charts and are used to calculate the capability indices Pp and Ppk. As for machine and process capability indices mentioned earlier, the Pp index describes variation with respect to the tolerance band and Ppk describes both variation and setting. As for Cmk and Cpk the lower value of Ppk is reported.

In some companies confusion can arise over how capability studies should by summarized using capability indices. To avoid any misunderstanding between the producer and the customer both should be in full agreement about how machine or process capability indices should be defined, determined and represented.

In carrying out capability studies or in the application of SPC companies whether large or small must be aware of the routes via which the products have been manufactured, including information on raw materials. With this knowledge an effective plan can be drawn up to show how the data is to be collected. Problems caused by combining data from measurements on a batch of nominally the same product but which has been produced by different sources can then be avoided. Examples of different sources producing an "identical" product include:

- Use of different batches or supplies of alloy ingot
- Sheet blanks or cut bar stock from different suppliers
- Multi-cavity or multi-impression moulds and dies
- Multi-spindle machines
- Separate machines of identical type
- Different combination of dies or moulds on different identical machines, etc.

In some cases we can recognize mixed work in a product batch by examining the shape of the resultant histogram, e.g. two peaks in a bimodal distribution, or by examining the straight line fit on a probability paper plot as in a machine capability study. In other cases we may believe that we have a non-normal distribution e.g. skew e.g. when measurements on some products from rogue cavities or positions in a mould have distorted the distribution. For example, in sand castings production these positions may arise due to:

- Original variation in mould or core-box dimensions from patternmaking or caused from damage, distortion or wear during use.
- Differences in the flow of sand around the pattern during filling and compression of a green sand mould or during filling/blowing and subsequent curing of a chemically bonded sand during core-making.

It is important to perform capability studies of the different combinations of dies or tooling sets and their host machines that are used to manufacture a given product so that combinations which give increased and possibly unacceptable variation can be identified and thus avoided. To avoid confusion and misconceptions in capability studies or in applying SPC it is paramount that systems for accurate recording of production information must be established. In seeking to improve capability small companies in general need to improve production record keeping so that raw materials, tooling and production variables used to produce a given product or part can be readily identified.

V. Concluding Remarks

The ongoing use of suitable control charts and assessment of process capability has proved to be one of the key steps in improving quality in manufacturing industries such as castings or forgings production where final product quality depends on a number of interrelated factors [7, 9-10].

Any manufacturing company must make products which are technically correct, are produced within budget, and are produced on time with a minimum wastage from defectives. In deciding which jobs to take on and how to cost them correctly without making a loss; small companies, in particular, must be able to recognize any limitations or deficiencies in their abilities and must be able to identify where improvements are needed. Small companies tend to have limited resources and difficulties in recruiting and training of workers. Nevertheless, with support from the topmanagement, suitable data collection procedures can be established and performance assessed using basic capability studies and introduction of suitable control charts. Progress can be made using simple manual plotting etc. on paper but where companies are confident in their understanding of the principles and application of capability studies and use of control charts, then it is likely to be more convenient to use a simple computer based system.

Other steps that can be taken include Process Mapping of procedures [11], use of Continuous Improvement techniques such as Plan – Do – Study – Act [12], Cause & Effects Analysis [13] and Pareto Analysis, etc. [14]. Table I summarizes the usefulness of some of these basic techniques.

TABLE I

SOME BASIC TECHNIQUES THAT CAN CONTRIBUTE TO IMPROVEMENTS

Technique	How this technique can help
Process flow charts	Show sequential stages of what is being done
Check and tally sheets	Record how frequently a particular event occurs
Bar charts (Histo-grams)	Give visual descriptions of pattern of variation
Scatter diagrams	Examine if there is a relationship between factors
Cause & effects analysis	Considers potential problems & possible causes
Pareto Analysis	Identifies the 2 or 3 main problems – "vital few"
Control charts	Differentiate between common andspecial causes – use statistics to control processes

REFERENCES

[1] W. Chamsuk, W. Fongsuwan, and J. Takala, "The Effects of R&D and Innovation Capabilities on the Thai Automotive Parts Industry Competitive Advantage: A SEM Approach". *Management and Production Engineering Review*, vol. 8, no. 1, pp. 100-112, Mar. 2017.

[2] P. Interakumnerd, and K. Technakananont. "Intra-industry Trade, Product Fragmentation and Technological Capability Development in Thai Automotive Industry". *Asia Pacific Business Review*, vol. 22, pp. 65-85, 2016.

[3] P. Sriboonlue, P. Ussahawanitchakit, and S. Raksong. "Strategic Innovation Capability and Firm Sustainability: Evidence from Auto Parts Businesses in Thailand". *Journal of Business & Retail Management Research*, vol. 10, no. 2, pp. 11-29, April. 2016.

[4] "Guidelines to Statistical Process Control" SMMT - The Society of Motor Manufacturers and Traders, London, 1986, 92 pp.

[5] "Statistical Process Control". Instruction Guide, Ford Motor Company, EU880, 1984, pp. 64.

[6] "Quality System Requirements QS-9000". First Edition (1994) August, Chrysler Corporation, Ford Motor Company, General Motors Corporation, 106 pp.

[7] J. T. H. Pearce. "Use of Statistical Process Control in Foundries". *Foundry (India)*, vol. 11, no. 5, pp. 19-28, Sep-Oct. 1999.

[8] "Measurement Systems Analysis MSA". Second Edition (1995) February, Chrysler Corporation, Ford Motor Company, General Motors Corporation, 120 pp.

[9] G.N. Booth. "Defining Quality Through SPC: Foundry Applications". Modern Castings (1985) Vol. May pp. 27-32.

[10] J. T. H. Pearce and P. Bhandubanyong. "Experience in the Use of Statistical Process Control (SPC) in Foundries". Proceedings of the 7th Asian Foundry Congress, Taipei, Taiwan 2001 pp. 591-601.

[11] D. Scrimshire. "Process Map Your Procedures". *Foundryman*, vol. 94, pp. 144-146, May. 2001.

[12] D. Scrimshire. "Training in continuous improvement techniques boost productivity". *Foundryman*, vol. 91 August pp. 260-262.

[13] J. T. H. Pearce. "An Introduction to Failure Modes and Effects Analysis". *Metal Casting Technologies*, vol. 61, pp. 20-24, June. 2015.

[14] "Tools and Techniques for Quality Management". SMMT - The Society of Motor Manufacturers and Traders (1991) London, 70 pp.

John T. H. Pearce holds a B.Sc. Hons. degree in Metallurgy (1967) and a Ph.D. in Wear of Abrasion Resistant Materials (1982), both awarded by the University of Aston in Birmingham, England.

Following research and production experience as a Technical Assistant at International Nickel, Rubery Owen Group and British Motor Corporation from 1962 to 1967, he joined British Cast Iron Research Association as a Research Metallurgist.

In 1970 until 1995 he was a Senior Lecturer in Metallurgy and Foundry Technology at Sandwell College FHE. In the West Midlands. He moved to Thailand in 1996 to be a Senior Metals Specials at the National Metals and Materials Technology Centre (MTEC) until he joined PIM in 2014 as a Lecturer in the School of Engineering. He has contributed to fourteen books/monographs, and is author/co-author of 160 articles, and more than 180 conference papers. His main research & consultancy interests include structure-properties relationships in metal castings, electron microscopy, wear and corrosion resistance, and quality management in metals production.

Dr. Pearce is a Past President of the Birmingham Metallurgical Association and in 1997 received the Voya Kondic Medal from the Institute of Cast Metals Engineers for services to education in the cast metals industry. In the UK. he was a Chartered Engineer, a Fellow of the Institute of Materials and a Member of the Institute of Cast Metals Engineers.

Paritud Bhandhubanyong holds a B. Eng. (1972) and M. Eng. (1976) (Industrial Engineering) from Chulalongkorn University, MBA (1976) from Thammasart University and D.Eng. (Metallurgy) in 1983 from the University of Tokyo. He joined the State Railway of Thailand as a junior engineer then moved to work as an instructor in the Faculty of Engineering, Chulalongkorn University. He was Head of Department of Metallurgical Engineering, Vice Dean of Planning and Development before joining the National Metal and Materials Technology Center as Executive Director. He then moved to be the Executive Director of the Technological Promotion Association Thai-Japan (TPA) before joining the Panyapiwat Institute of Management as Executive Director in the office of the President and acting Head of Department of Automotive Manufacturing Engineering. His research interest included Casting Technology, TQM, TPM, TPS. and work-based education (WBE) practices. His recent papers and publication included a chapter in the Report on ASEAN Automotive Industry 2016 (in Japanese) , Business Continuity Management (TPA, 2015) and a paper on WBE presented at ISATE 2016.

Dr. Paritud is a member of the Japan Foundry Engineering Society, The Iron and Steel Institute of Japan, former Chairman of the Foundation of TQM Promotion of Thailand, committee member of the Standard and Quality Association of Thailand, advisor to the Thai Foundry Association of Thailand and the Materials and Corrosion Society

Influence of Fiber Length of the Fractionated Pulp and its Fiber Swelling Capacity on Compressive Resistance and Other Strength Properties of Corrugating Medium Handsheet

Wiroj Savangsrisutikun* and Phichit Somboon

Department of Forest Products, Kasetsart University, Bangkok, Thailand
E-mail: Wirojm2533@hotmail.com*

***Abstract*—The objective of this research work was to understand the influence of length and swelling capacity of fractionated pulp fibers on compressive resistance of corrugating medium handsheet and its other strength properties. In this work, the three length fractions of pulp fibers with various degrees of fiber swelling, which was measured with the water retention value (WRV) test, in the range of 1.20-1.70 g/g were used as the fiber samples for making the handsheet with a grammage of 90 g/m^2. These fibers were prepared by fiber fractionating three samples of unbleached softwood kraft pulp with the different freeness levels with the Bauer-McNett classifier. The results showed that compressive resistance of the handsheet, which was measured with the Concora test (CMT), was not increased with an increase in the fiber length of fractionated pulp, but increased significantly with increasing the fiber swelling capacity. On the other hand, the tear strength seems not to be affected by the fiber swelling capacity, but to be significantly affected by the fiber length of fractionated pulp. Other strength properties of the handsheet such as tensile and burst strength were found to be significantly related to the length and swelling capacity of the fibers.**

***Index Teams*—Compressive resistance, strength properties, corrugating medium handsheet, fiber length, fiber swelling**

I. Introduction

Nowadays, corrugated container is one of the most widely used packaging materials in every nearly industry worldwide. This success is because of its versatile, serviceability, stacking strength and low cost of production. Corrugated container is also lightweight, eco-friendly and recyclable, as well as has excellent printability for branded packaging. In Fig. I, a common feature of corrugated container is presented.

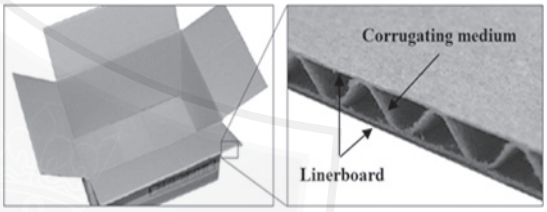

Fig. I. Corrugated paperboard container and its structural components

As shown in Fig. I, corrugated container is made primarily from corrugated paperboard that consists of linerboard and corrugating medium. Linerboard is generally referred to as heavyweight grades of paperboard used as the inner and outer facings of corrugated paperboard. The corrugated medium is a lightweight paperboard that is formed into the wave shape to be used as the corrugated medium layer of the board [1, 2, 3].

Corrugating medium is a critical component of corrugated board production because without the medium, the product would be either a cardboard box or a paper bag. Typically, it has function of contributing the structural rigidity of corrugated board and promoting the cushion characteristic of containers [4, 5]. For this reason, strength properties are very important for the performance quality of corrugating medium [6]. One of the most important strength properties of corrugating medium is compressive resistance which is measured with corrugating medium test or Concora test [3, 6]. The Concora test is a measure of the compression of the paper after corrugating [7]. Fig. II demonstrates the test of compressive resistance of corrugating medium.

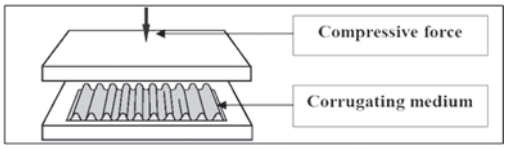

Fig. II. Corrugating medium test

Generally, the result from the Concora test suggests that the compressive resistance depends mainly on the quality of paper material used in the corrugating plant [7]. Because paper is a thin sheet material that is mainly made up of an interlocking network of wood pulp fibers, its quality is basically determined by properties of the fibers used in the papermaking process. The important properties are the morphological properties of pulp fibers such as fiber length, fiber width and cell wall thickness [8, 9, 10]. Of these, the length is one of the most important characteristics of pulp fibers, which is closely related to paper strength properties and is very often used as a measure of pulp quality in the paper industry [11, 12, 13, 14]. In addition to fiber length, fiber swelling capacity, or the fiber ability to retain water in the cell wall, is another fiber property which has long been considered to be an important property in papermaking. It has been reported that the swelling capacity of fibers has a great impact on sheet consideration and interfiber bonding [15, 16, 17].

However, there is noclear information about the influence of fiber properties mentioned above on compressive resistance of corrugating medium. This can cause problems in controlling the stock quality for the corrugating paper, and consequently the performance quality of corrugated medium will be affected. Thus, the aim of the present study was to understand effect that fiber length and swelling capacity of fibers have on compressive resistance of corrugating medium paper. In addition to the compressive resistance, the effect of those fiber properties on other strength properties of the paper was also investigated in this work.

II. Materials and Methods

A. Raw material

The fiber samples used in this study were the three length fractions of pulp fibers, consisting of long, middle and short fraction. The each fraction also contained the three different degrees of fiber swelling. These pulp fibers were prepared by fiber fractionating unbleached softwood kraft pulps with the different freeness levels of 550, 350 and 150 ml (Canadian Standard Freeness-CSF).

B. Fiber fractionation

Fiber fractionation was carried out by using a Bauer-McNett type classifier at the laboratory of pulp and paper technology, department of forest product, faculty of forestry, kasetsart university, Thailand. In the fractionation, the pulp (10.0 g, oven dried) in water of 1000 mL was used. The fractionation was performed using screens of 14-, 28-, and 200-mesh (Tyler standard screen scale) for 20 min. After 20 min, the fibers retained on 14-mesh screen were defined as long fiber fraction, the fibers passed 14-mesh screen but retained on 28-mesh screen were middle fiber fraction, while short fiber fraction was the fibers that were passed 14- and 28-mesh screen but retained on 200-mesh screen.

C. Handsheet forming

Handsheets were prepared at a grammage of 90 g/m^2, and formed in a laboratory handsheet former according to the ISO 5369 standard method. Before the paper strength tests were performed, all the handsheets were conditioned at 23^{o}C and 50% relative humidity in accordance with the ISO 187 standard method for at least 24 h.

D. Pulp and paper properties measurements

In this work, swelling capacity of the fibers was measured with the water retention value (WRV) test in accordance with the SCAN-C 62:00 standard method. Morphological characteristics of the fibers such as length, width and coarseness were measured by using a Fiber Quality Analyzer according to the ISO 16065-1 standard method. Compressive resistance of the corrugated medium handsheet was measured with the concora medium test (CMT) according to the ISO 7263 standard method. The in-plane tensile properties of the sheet including tensile stiffness and tensile strength was measured and calculated following the ISO 1924-2 standard method. The tear strength was measured using an Elmendorf tear tester according to the ISO 1974 standard method. Burst strength of the sheet was measured according to the ISO 2758 standard method. The interfiber bonding strength of sheet was measured by using the inter bond tester (Scott type) in accordance with the TAPPI T 569 om-14 standard method.

E. Data analysis

The data was analyzed using one-way analysis of variance. Duncan's new multiple range test, at 95% confident level, was used for comparing and grouping the mean values.

III. Results and Discussion

F. Pulp properties of the fiber samples

In this work, three samples of the softwood pulp (SW) with a pulp freeness of 550, 350 and 150 ml CSF were used as the raw material for preparing the fiber samples with various lengths and swelling capacities. Table I shows a summary of properties of the pulp fibers obtained from fiber fractionation of the SW pulp in the Bauer-McNett classifier that was performed using screen of 14-, 28- and 200-mesh. Results from Table I show that there was no significant difference in the fiber length and fiber width of the fractionated pulp in the same length fraction. The average fiber length for long fraction was about 3.01 mm, while the middle and short fraction was about 2.09 and 1.14 mm, respectively. The mean width of the fibers was about 42.59 μm for the long fraction,

41.48 µm for the middle fraction and 38.58 µm for the short fraction. Additionally, the results indicate that the swelling capacity, which was measured with the WRV test, of each fiber sample used in this study had statistically significant difference. Swelling degree of the fractionated pulp was in the range between 1.20 and 1.70 g/g. Based on the results obtained, the coarseness value, which indicates the cell wall thickness, showed significant difference in the pulp having different length fraction. The fractionated fibers with the longest length had the highest value of coarseness. As can be observed, the coarseness value was decreased as the swelling capacity of fractionated pulp increased. This result could be explained by the water retained by capillarity inside the lumens. When the fibers contain more total volume of lumen (lower wall thickness), they have higher WRV value.

Table I
PULP PROPERTIES OF THE FIBER SAMPLES

Raw materials	Length fraction	Properties of the fractionated fibers			
		Length (mm)	Width (µm)	Coarseness (mg/g)	WRV (g/g)
SW500	Long (R14)	3.01a	42.93a	0.278a	1.22i
SW350	Long (R14)	3.00a	42.63a	0.272b	1.30h
SW150	Long (R14)	2.99a	42.20a	0.263c	1.35f
SW500	Middle (P14/R28)	2.10b	41.53b	0.216d	1.34g
SW350	Middle (P14/R28)	2.10b	41.47b	0.204e	1.38d
SW150	Middle (P14/R28)	2.08b	41.43b	0.199f	1.46c
SW500	Short (P14,28/R200)	1.15c	38.83c	0.180g	1.35e
SW350	Short (P14,28/R200)	1.14c	38.60c	0.164h	1.58b
SW150	Short (P14,28/R200)	1.14c	38.30c	0.155i	1.70a

G. Mechanical properties of the handsheets

Fig. III shows the effect of average fiber length and fiber swelling capacity, which was measured with the WRV test, of the fractionated pulp on the compressive resistance of the handsheet, which was measured with the Concora test (CMT). The figure shows that compressive resistance of the handsheet was not increased with increasing the average fiber length of fractionated pulp. It seems that the CMT value was mainly depended onthe fiberswelling capacity. As reported by Whitsitt and Sprague [18], the compressive resistance (CMT) is a function of elastic modulus of the sheet. In this study, it was found that when the average length of pulp fibers increased, the specific elastic modulus of the sheets (elastic modulus divided by sheet density)was not increased, as shown in Fig. IV. This phenomenon could be explained from Fig. V. In Fig. V, the effect of average fiber length of fractionated pulp and itsfiber swelling capacity on the bonding strength, which is considered as the main factor controlling the elastic modulus of sheet [19], is illustrated. As shown in Fig. V, the bonding strength of handsheets was significantly decreased when the average fiber length of fractionated pulp was increased. This might be because the fractionated pulp with longer length had the higher coarseness value compared to the fibers with shorter length (Table I). The high coarseness value usually results in the fibers with low conformability and poor bonding ability, and therefore the bonding strength is decreased. Based on these results, it could be concluded that the swelling capacity of fractionated pulp was a main contributing factor of compressive resistance of the corrugating medium handsheet.

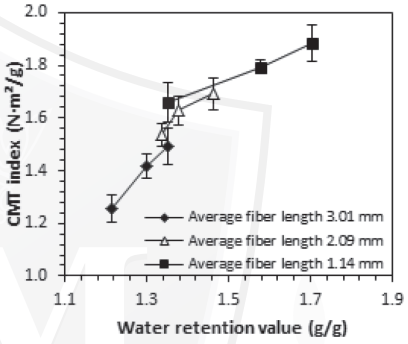

Fig. III. Compressive resistance (CMT) as function of fiber length and fiber swelling capacity of the fractionated pulp

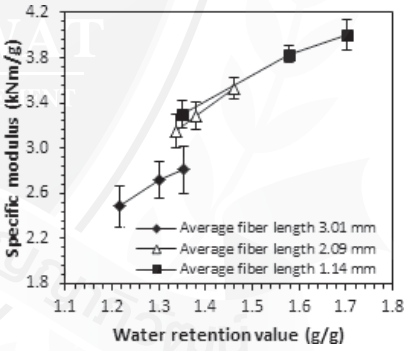

Fig. IV. Effect of fiber length and fiber swelling capacity of the fractionated pulp on the specific modulus of handsheets

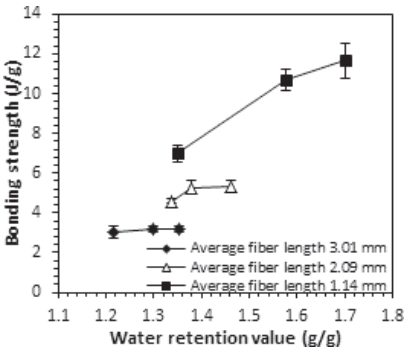

Fig.V. Effect of fiber length and fiber swelling capacity of the fractionated pulp on the interfiber bonding strength of handsheets

Tensile strength is one of the most important strength properties of paper and paperboard, which mainly depends on fiber bonding, fiber length and intrinsic fiber strength [19]. Therefore, it was found that when the swelling capacity of fractionated pulp was increased, the tensile index of handsheets was significantly increased (Fig. VI), which was due to its positive effect on the interfiber bonding strength in paper (Fig. V). Moreover, it could be observed from Fig. VI that at the lowest swelling degree, the long fiber fraction did not provide higher tensile strength of the sheet than the middle and short fiber fraction. This might indicate that the average length of pulp fibers had less effect on the sheet strength when the fibers had the poor bonding potential. At the similar swelling capacity, the fractionated pulp with longer fiber length generated the handsheets with superior tensile strength. This demonstrated the long fiber fraction had higher resistance to be deformed plastically under tensile force compared to the middle and short fiber fraction (Fig. VII)

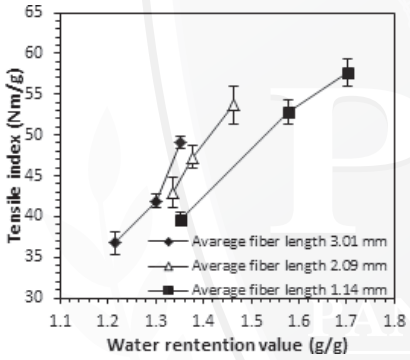

Fig.VI. Effect of fiber length and fiber swelling capacity of the fractionated pulp on the tensile strength of handsheets

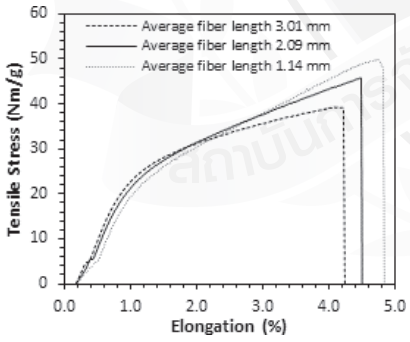

Fig. VII. Load-elongation behavior of the sheets made from the three different length fraction of fractionated pulp with similar swelling degree

Fig. VIII shows the effect of length and swelling capacity of the fractionated pulp fibers on the burst index. Basically, the burst strength depends on the fiber length and fiber bonding. Hence, it was not surprising that the burst index of handsheets was found to be greatly improved with increasing the fiber length of fractionated pulp and its swelling capacity.

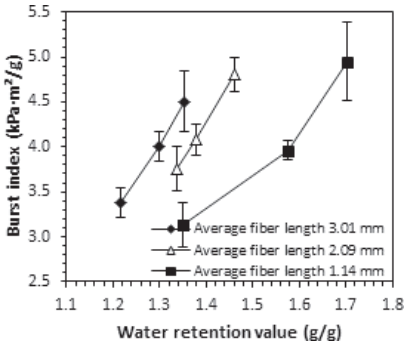

Fig.VIII. Effect of fiber length and fiber swelling capacity of the fractionated pulp on the tensile strength of handsheets

Fig. IX shows the effect thatthe fiber length and fiber swelling capacity of fractionated pulp have on the tear index. According to Paavilainen[13], tearing resistance of paper is a function of intrinsic fiber strength, fiber length and bonding degree of fibers. Therefore, the handsheets made from the long fiber fraction had higher tear index compared to those made from the middle and short fiber fraction, which was becausethe long fiber fraction had higher length and coarseness (Table I). Although Paavilainen [13] has explained that tear strength is also related to the fiber bonding degree in paper, in the present study we found that the increase in the swelling capacity of fractionated pulp did not result in the sheets with increased tear strength. This means that the fiber length had much stronger impact on the tear index more than the fiber swelling capacity did.

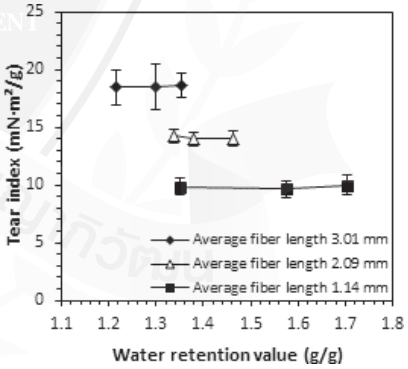

Fig. VIII. Effect of fiber length and fiber swelling capacity of the fractionated pulp on the tensile strength of handsheets

IV. Conclusion

In this study, effect of fiber length and fiber swelling capacity of the fractionated SW pulp on compressive resistance and other mechanical properties of corrugating medium handsheet was examined. The results showed that compressive resistance of the corrugating medium handsheets, which was measured with the Concora test, was not increased with increasing the average fiber length of fractionated pulp. This was because increasing the average length of fractionated

fibers did not result in the increased elastic modulus, which is one of the effective parameters for the compressive resistance (CMT). Thus, the CMT of handsheets was found to bemainly dependent on the fiber swelling capacity of fractionated pulp. On the other hand, tear strength of the handsheet was found not to be dependent on the fiber swelling capacity, but to be dominantly controlled by the fiber length of fractionated pulp. Other strength properties of handsheets such as tensile and burst strength were found to be affected significantly by the fiber length and fiber swelling capacity of fractionated pulp.

V. Acknowledgements

The authors would like to thank Graduate School, Kasetsart University for providing part of the funding for this research. The experimental work of this research was carried out at Laboratory of Pulp and Paper Technology, Department of Forest Products, Faculty of Forestry, Kasetsart University which is gratefully acknowledged.

References

[1] R. N. Dehankar, A. M. Langde, S. Siddiqui, and D. J. Tidke, (2014) "Review on Paper Corrugated Box Manufacturing used in Goods Packaging," *IOSR-JMCE*, pp. 28-30. Available:http://www.iosrjournals.org/iosrjmce/papers/ICAET-2014/me/volume-6/7.pdf?id=7622

[2] R. E. Popil, "Overview of Recent Studies at IPST on Corrugated Board Edge Compression Strength: Testing Methods and Effects of Interflute Buckling," *Bio Resources*, vol. 7, no. 2, pp. 2553-2581, May. 2012.

[3] T. Watkins, "Corrugated board packaging," in *Packaging Technology Fundamentals, Materials and Processes,* A. Emblem and H. Emblem, Eds. Woodhead Publishing, 2012, pp. 240-261.

[4] M. A. Sek and V. Rouillard,"Behaviour of multi-layered corrugated paperboard cushioning systems under impact loads,"*Applied Mechanics and Materials*, vol. 43, no. 4, pp. 383-388, Oct. 2005.

[5] M. A. Sek, V. Rouillard, S. Crawford, and H. Tarash, "Enhancement of cushioning performance with paperboard crumple inserts,"*Packaging Technology and Science*, vol. 18, no. 5, pp. 273-278. Jun. 2005.

[6] S. P. Gurav, A. Bereznitski, A. Heidweiller, and P. V. Kandachar, "Mechanical properties of paper-pulp packaging," *Composites Science and Technology*, vol. 60, no. 9, pp. 1325-1334, Jul. 2003.

[7] J. Poustis, "Corrugated fibreboard packaging," in *Paper and Paperboard Packaging Technology,* M. J. Kirwan, Ed. Wiley-Blackwell, 2005, pp. 317-371.

[8] U. B. Mohlin, J. Dahlblom, and J. Hornatowska, "Fiber deformation and sheet strength," *Tappi J,* vol. 79, no.6, pp. 105-111, Jun. 1996.

[9] P. Kärenlampi and Y. Yu, "Fiber properties and paper fracture – fiber length and fiber strength," in *The Fundamentals of Papermaking Materials, Transactions of the 11th Fundamental Research Symp.* Cambridge, England, 21-26 Sep. 1997. Pira, UK, 1997. vol 1, pp. 521-545.

[10] A. Moral, M. C. Monte, E. Cabeza, and A. Blanco. "Morphological characterization of pulp to control paper properties," *Cellulose Chemistry and Technology,* vol. 44, no. 10, pp. 473-480, Nov. 2010.

[11] E. Saharinen, S. Heinemann, T. Hjelt, and J. Sirvio, "Fiber length and sheet properties: some new considerations," PTS Pulp Symposium.Dresden, Germany, Nov. 24-25, 2009.

[12] H. Yan, B. Norman, T. Lindstrom, and M. Ankerfors, "Fiber length effect on fiber suspensionflocculation and sheet formation," *Nord Pulp Pap Res J*, vol. 21, no. 1, pp. 30-35, Jan. 2006.

[13] L. Paavilainen, "Influence of fibre morphology and processing on the softwood sulphatepulp fibre and paper properties," Ph.D. dissertation, Helsinki University of Technology, Espoo, Finland, 1993.

[14] L. Paavilainen, "Influence of morphological properties of softwood fibres on sulphatepulp fibre and paper properties," in *International Paper Physics Conference*, Kona, Hawaii, 1991, pp. 383-395.

[15] P. Przybysz1, M. Dubowik, M. A. Kucner, K. Przybysz1, and K. P. Buzała1, "Contribution of Hydrogen Bonds to Paper Strength Properties," *PLOS ONE,* vol. 11, no. 5, May. 2016.

[16] A. Vainio, H. Paulapuro, "Interfiber bonding and fiber segment activation in paper," *BioResources,* vol. 2, no. 3, pp. 442-458, Aug. 2007.

[17] F. J. Schmied, C. Teichert, L. Kappel, U. Hirn, W. Bauer, and R. "What holds paper together: Nanometre scale exploration of bonding between paper fibres,"*Sci. Reports*, Aug. 2013.

[18] J. W. Whitsitt and H. C. Sprague, "Optimization of machine properties for compressive strength," Project 2695-22, report one: a progress report to the Fourdrinier Kraft Board Group of the American Paper Institute. Available: https://smartech.gatech.edu/handle/1853/702.

[19] E. Retulainen, K. Niskanen, and N. Nilsen, "Fiber and bonds," in *Paper Physics,* vol. 16, pp. 54-87, 1998.

Wiroj Savangsrisutikun, Now, I am a graduate student in Wood and Paper Industrial Technology Program, Department of Forest Products, Faculty of Forestry, Kasetsart University. I was received B.S. (Pulp and Paper Technology) at Kasetsart University, Thailand in 2012.

Phichit Somboon, Asst. Prof. Now, he is Associate Dean for Education, Faculty of Forestry, Kasetsart University. He was received B.S. (Forest Products) from Kasetsart University, Thailand. M.S. (Paper Technology) Helsinki University of Technology, Finland. D.Sc. (Tech). Helsinki University of Technology, Finland.

Investigation of Copper Anode Treatment

Jarunee Kraikaew[1] and Brajendra Mishra[2]

[1]Regulatory Technical Support Division, Office of Atoms for Peace, Bangkok, Thailand
[2]Department of Metallurgical and Materials Engineering,
Colorado School of Mines, Golden, CO, USA
E-mail: jarunee.k@oap.go.th, bmishra@mines.edu

Abstract— **This research was performed to study the electrochemistry of copper anode treatment of Coors beer, manufactured from Coors Brewing Company, to capture the trace amounts of sulfur. The relationship between electrode surface area, electrode separation or electrode gap, copper dissolution and current/voltage applied was investigated using small scale electrochemical cell. The optimum conditions, which limited the copper dose approximately 30 ppb to 50 ppb in the beer stream for removing the trace amounts of H2S and other sulfur compounds, were determined. The small scale electrochemical cell was designed and set up, as well as the continuously copper concentration analysis system by Ion Analyzer. The compositions of corrosion scale from Coors copper prototype electrode was analyzed by X-ray diffraction method. The data interpretation and analysis was accomplished via Microsoft Excel spreadsheet using desktop computer.**

The experimental results showed that; 1) Electrode separation of "¾-in to 1-in" was optimum for high current efficiency but the gap "¾-in" was more practical; 2) The minimum current was supposed to be 0.5 A, which maintained the copper dose in the range of 35 ppb to 40 ppb; 3) The current density change was higher with the higher surface areas; 4) Electrode fouling was caused from both sulfides and oxides of copper, which were mixed together in corrosion scale; and 5) Formation of copper sulfide was preferred over copper hydroxide precipitation.

***Index Teams*: beer stream, copper dose, electrochemistry, H2S, sulfur capture.**

I. Introduction

This research was performed in 2000-2001 in Corrosion Laboratory, Department of Metallurgical and Materials Engineering (MME), Colorado School of Mines (CSM), CO, USA, as a project to support the beer manufacturing of Coors Brewing Company. It was aimed to study the electrochemistry of copper anode treatment of beer to capture the trace amounts of sulfur. The effects of electrode separation and electrode surface area on the efficiency of copper dosing of the beer stream were evaluated. The electrolytes, water and beer, were provided by Coors Brewing Co., which was the sponsor for this project. The main objectives of this research were;

1) To determine the relationship between electrode surface area, electrode gap, copper dissolution and voltage applied using small scale electrochemical cell in order to apply to an existing copper anode prototype for scale up.

2) To investigate the optimum conditions that allow approximately 30-50 ppb [Cu] of copper dose to the beer stream for removing the trace amounts of H2S and other sulfur compounds which contributed to an off-state.

II. Experimental

A. Process equipment set-up

The electrochemical cell was designed for operating in both static and circulating modes [1]. The electrode holder racks were installed on the plexiglas cover where some holes were drilled for the pH/mV probe, temperature probe, and PVC pipes. Two PVC pipes were inserted through the holes on this cover to support the plastic tubes from the circulation pump and the small syphon pump.

The copper plate was cut into two copper electrodes, each of 10 cm x 20 cm. The hanging holes were drilled on the top and the paint was sprayed to coat all surfaces except 10 cm x15 cm area. To install the copper electrodes to the electrochemical cell, the copper electrodes were hooked with the electrical wires from the cover. The distance gap was adjusted from the holder racks and by bending electrical wires. The electrical wires length in the electrochemical cell was also adjusted, to maintain the immersion depth of both copper electrodes in the electrolyte.

The PHI-40, Ion Analyzer, was applied to measure pH/mV and temperature of the electrolyte continuously while the electrochemical cell was in operation. The solution output from the small circulation pump, using the old model of Cole-Palmer thermoregulator, was separated into two lines. One was by-passed back to the thermoregulator storage tank. The solution in another line flew through the rotameter to the electrochemical cell. The volume in the electrochemical cell was

controlled from the rotameter, the electrolyte height, and the small syphon-pump that recycled solution back to the thermoregulator storage tank. The photograph of this equipment set-up is shown in Fig. I.

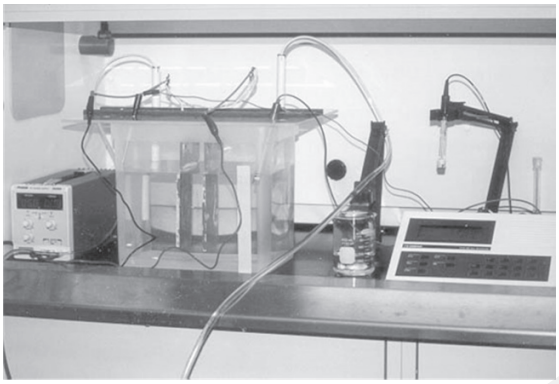

Fig. I. Electrochemical cell set-up.

B. Preliminary Testing Procedures

1) Estimation of the voltages and the amperes applied

The small electrochemical cell, static mode, was set up using 500 ml beaker. The cathode and anode, which were the small copper strips coated one face with spray paint, were connected to the DC power source. The following steps were carried out;

a. Trial and error test was run using the tap water electrolyte and the high voltage of over 20 volts (V). The deep gelatinous blue precipitate [2] of $Cu(OH)_2$ occurred on the anode rapidly and the gas bubbled on the cathode. The voltage was lowered to 5 V and the electrochemical cell was operated for 1.5 h. The blue precipitate occurred slightly and there was no appreciable weight loss.

b. The trial and error test was repeated using Coors-A-Light water with 5 V and 1.5 amperes (A) maximum. The blue $Cu(OH)_2$ precipitate was observed at the conditions of 1.5 Wh and higher. The weight loss was plotted as a function of power supplied in 1.5 h. The graphical presentation is illustrated as Fig. II. The photograph of the blue gelatinous $Cu(OH)_2$ precipitate occurred, is shown in Fig. III.

The experimental results indicated that in this cell, the limiting current of the electrochemical process was about 0.5 A under the conditions applied.

List of experimental details in Fig. II.				
V	*A*	*P, Wh*	*W, g*	*Note*
5	1.5	11.25	0.0112	$Cu(OH)_2$ precipitated.
5	0.5	3.75	0.0097	$Cu(OH)_2$ precipitated.
3	0.5	2.25	0.0064	$Cu(OH)_2$ precipitated.
2	***0.5***	***1.5***	***0.0018***	***Slightly $Cu(OH)_2$ occurred.***
1	0.5	0.75	0.0009	No precipitate observed.
W = Anode weight loss *P = Power applied, Wh*				

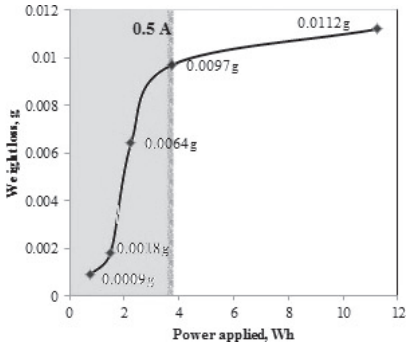

Fig. II. Plot of anode weight loss as a functionof the power applied.

Fig. III. The blue gelatinous $Cu(OH)_2$ precipitate from different power applied.

2) Estimation of the immersion depth and the distance gap

The copper electrodes were arranged in the electrochemical cell with Coors-A-water as an electrolyte. The experiments were carried out in static condition with two immersion depths of 13.5 cm and 7.0 cm. The electrode gaps tested were 3-in, 2-in, 1-in, and ¾ -in. The current setting was 1 A maximum and the maximum voltage applied was 5 V.

The voltage (V) applied was decreased and the cell current (I) readings were recorded from DC power source. The current density was calculated by dividing the cell current with the electrode surface area (A_E). The relationship between the current density, the voltage applied, the electrode gap, and the immersion depth are illustrated in Fig. IV. and Fig.V.

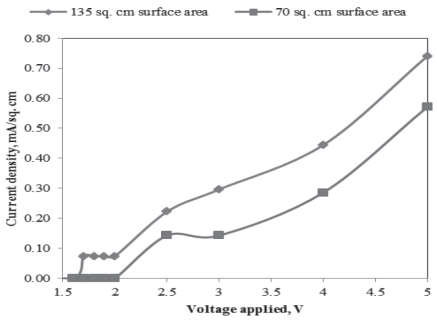

Fig. IV. The current density changes with different surface areas at ¾-in electrode gap as a function of the voltage applied.

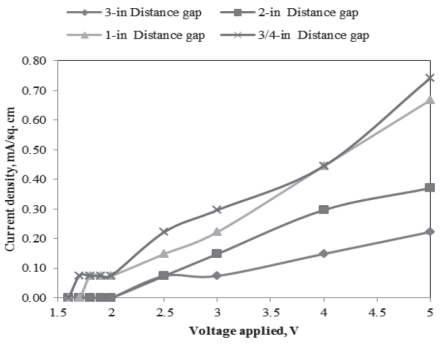

Fig. V. Plot of the current density as a function of voltage applied for the 135 cm2-surface areas.

3) Investigation of the difference between tap water and Coors-A-water electrolyte

The electrochemical cell was operated with 150-cm^2 copper electrodes in static condition. The voltage was increased, from zero to 5 V for Coors-A-water electrolyte, and from zero to 15 V for tap water electrolyte. The electrode gap was 2.5-in for Coors-A-water electrolyte and 2.75-in for tap water electrolyte.

At the same voltage applied, 5 V, the cell current reading was 0.03 A for tap water electrolyte. It was lower than the cell current reading of 0.05 A for Coors-A-water electrolyte, although the electrode gap was ¼ -in higher (Δ = 2.75– 2.5 = 0.25-in or ¼-in). This was due to higher conductivity of Coors-A-water than the tap water.

C. Analysis Procedures

1) Copper ion concentration analysis study using PHI-40 and Cu-ion selective electrode

Omega PHI-40 Ion Analyzer had the capability to measure pH, millivolts (mV), concentration, and temperature. The pH/mV mode and the ion-mode were applied for the ion concentration analysis. In order to analyze the copper ion concentration in the electrolyte, the Cole-Palmer copper ion selective electrode was connected to PHI-40.

The preliminary chemical analysis study was performed both in mV-mode and ion-mode following the operating procedures of PHI-40 and Cu-ion electrode. Despite of the low copper concentration in the process electrolyte, it was necessary to investigate the analysis method for copper concentration, which was lower than 0.6 ppm, for accuracy and precision. The chemical analysis was achieved using 100-ml solution, and then ionic strength adjuster (ISA) or low level ISA was added, followed with uniform mixing by magnetic stirrer. The Cu-ion electrode and the temperature probe were put in the solution. It took 15 min to 1 h for the stabilized millivolt (mV) reading depending on the concentration of copper in the solution.

The rough estimation of copper concentration was investigated using ion-mode. The actual concentration was measured with mV-mode from the calibration curve of the standard solutions in the same range of mV-readings. The solution matrix for the standards was needed to be the same as the sample solution matrix.

The accuracy from the low level copper concentration analysis was 14.34 ppb using 10-ppb standard solution, de-ionized water matrix. For Coors-A-water matrix, the accuracy was 0.1174 ppm from 0.1 ppm standard copper solution. For the low 10-ppb concentration, the deviation is 43.4%. For the higher 0.1-ppm or 100-ppb concentration, the deviation is 17.4%. The higher the concentration, the more the accuracy.

The copper concentration in Coors-A-water after passing the current from the above preliminary test was measured by this procedure. Its concentration was 1378.69 ppb or 1.38 ppm.

2) X-ray diffraction analysis of corrosion scale from copper electrode

The black corrosion scale from Coors copper prototype electrode was scrubbed, filtrated, rinsed with de-ionized water and acetone. After drying, it was grounded with ceramic mortar. The scale analysis was achieved using Rigaku X-ray diffraction equipment with the following operating conditions.

The intensities of various peaks from the XRD results were compared with the theoretical intensity in JPDS-International Centre for Diffraction Data at the same d-spacing value. The analytical results showed that the oxide and sulfide compounds of copper and iron were mixed together. They were β-Cu_2S, CuS_2, CuS, Cu, CuO, Cu_2O, Fe_2O_3, FeO, and FeS.

The oxides occurred from the reactions of the ions of copper and irons with oxygen dissolved in the beer stream. The corrosion of the steel pipes caused the iron ions to the solution. The trace amounts of H_2S and other sulfur compounds in the beer stream formed sulfide compounds with ions of copper and iron.

From the anode reaction, the copper ion was supposed to be Cu^{2+} more than Cu^{1+}. Therefore, the main copper sulfide corrosion scale should be CuS_2 (black) and CuS (dark blue).

III. Experimental Runs and Results

A. Test Runs

The test runs were operated in both static and circulated-electrochemical cell. The electrolytes used in these experiment runs were;

a) Spoiled Coors-Light beer;
b) Fresh Coors-Light beer;
c) The mixed beer from the fresh and used electrolyte; and
d) The de-ionized water.

The copper electrodes were weighed before and after each electrochemical cell. The total exposure time was 1 h and the samples were taken every 15,

30, and 60 min. The voltage applied was 5 V with 1 A current maximum. The electrode gap fixed was 1.5-in and the immersion surface area was 9.5 cm × 10 cm. for Experiment #1 and 10 cm × 15 cm for Experiments #2, 3, and 4.

Experiment 1

The immersion depth was only 9.5 cm and then the surface area was only 9.5 cm x10 cm or 95 cm^2. Three samples, 100 ml each, were pipetted at 15, 30, and 60 min. Assumed that the amount of the samples pipetted was neglected compared with the total volume of the electrolyte in the electrochemical cell.

The pH and mV of this spoiled beer before passing the current was 3.899 at 21.6°C and 170.1 mV at 21.8°C, respectively. The pH increased from 4.157 at 21.2°C to 4.242 at 21.3°C in 60-min operating time. The cell current reading reduced from 0.11 A at starting to 0.10 A, in 60 min. The anode weight loss was 1 g using rough weight balance.

The beer was spoiled by bacteria before and it looked deep yellow, high turbidity and viscosity. There was a problem analyzing with mV-mode because of the lower pH occurring from bacteria reactions. *This experiment was implemented for the first trial and error test to continue for the next runs, # 2, 3, and 4 (Table I).*

TABLE I
EXPERIMENTS 2, 3, AND 4

Operation conditions	**Exp. Run # 2**	**Exp. Run # 3**	**Exp. Run # 4**
Run mode	Static	Circulating	Circulating
Starting electrolyte	Fresh Coors beer	Fresh Coors beer mixed with Run # 2-used electrolyte	De-ionized water
pH/mV and cell current reading of the starting electrolyte	• pH = 4.335 at 21.0 °C • Conductivity 145.3 mV at 21.0 °C • Cell current = 0.13 A	• pH = 4.406 at 22.0 °C • Conductivity 141.0 mV at 22.0 °C • Cell current = 0.14 A	• pH = 5.949 at 21.3 °C • Conductivity 52.1 mV at 21.3 °C • Cell current < 0.01 A
Operating conditions	• 5 V, 1 A • 1.5-in distance gap • 10 cm × 15 cm or 150 cm^2 immersion surface area • 1-h exposure time • 10-L approximate beer volume	• 5 V, 1 A • 1.5-in distance gap • 10 cm × 15 cm or 150 cm^2 immersion surface area • 1-h exposure time • 12-L approximate beer volume in electrochemical cell and circulator. • 6 + 1 gph input flowrate	• 5 V, 1 A • 1.5-in distance gap • 10 cm × 15 cm or 150 cm^2 immersion surface area • 1-h exposure time • 12-L approximate beer volume in electrochemical cell and circulator. • 6 + 1 gph input flowrate
Anode weight loss (Same cathode weight)	*0.16 g*	*0.14 g*	*0.11 g*
pH/mV and cell current reading of 60-min electrolyte	• pH = 4.428 at 21.3 °C • Conductivity 138.6 mV at 21.3 oC • Cell current = 0.13 A	• pH = 4.483 at 22.7 °C • Conductivity 137.3 mV at 22.7 °C • Cell current = 0.13 A	• pH = 6.213 at 21.8 °C • Conductivity 37.4 mV at 21.8 °C • Cell current < 0.01 A

After shut down the current, pH/mV of the electrolyte from Exp. Run # 2 and Exp. Run # 3 were measured again. It was found that pH decreased but mV increased. The copper electrodes were pulled out, cleaned, and weighed. The photograph of the copper electrodes after experimental run is sown in Fig. VI. The cathode surface was bright because of the hydrogen gas occurred but there were some dark dirty areas. They might be foul from some oxide or sulfide scales. The anode surface looked deep golden brown after elimination of Cu^{2+} to the electrolyte.

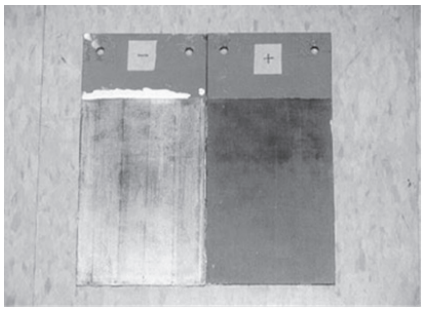

Fig. VI. Copper electrode surfaces after current passing.

In order to investigate the phenomenon happened, pH/mV of the Exp. 4-solution electrolyte after shutting down the current was measured in half an hour. *Plots of pH/mV of Exp. 2-4 vs exposure times were illustrated in Fig. VII, VIII, and IX.* The concentrations of copper in the input, output, and every 15, 30, and 60 min were analyzed using PHI-40 with Cu-selective electrode in ion-mode and mV-mode. *The copper concentration profiles of 60-min exposure time were illustrated as in Fig. X, XI, and XII.*

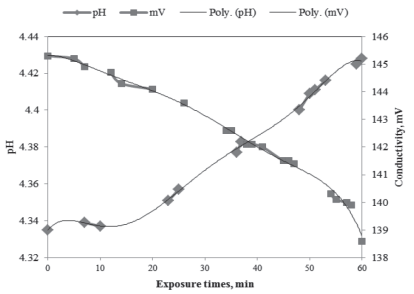

Fig. VII. Plot of pH and conductivity as a function of exposure time in the static electrochemical cell using fresh Coors Light beer as an electrolyte.

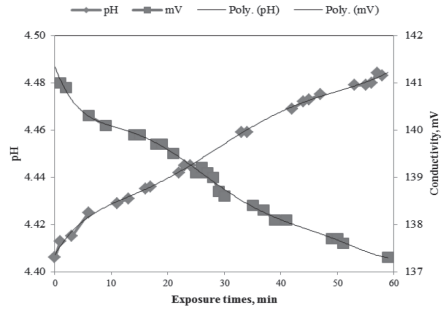

Fig. VIII. Plot of pH and conductivity as a function of exposure time in the circulated-electrochemical cell using mixed electrolyte from fresh Coors Light beer and Exp.2-used Coors Light beer electrolyte.

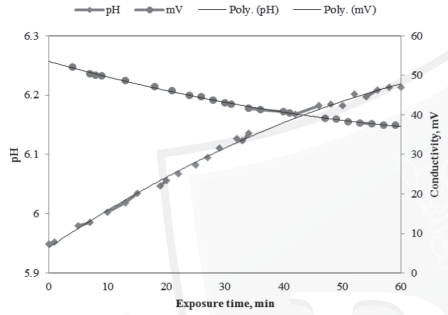

Fig. IX. Plot of pH and conductivity as a function of exposure time in a circulated-electrochemical cell using de-ionized water as an electrolyte.

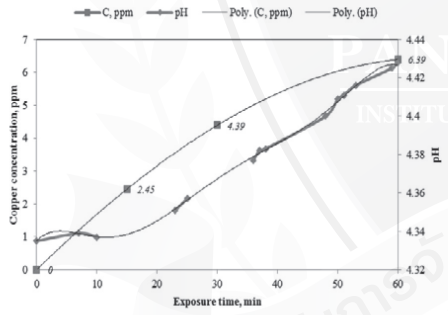

Fig. X. Plot of copper concentration profile and pH as a function of exposure time in static electrochemical cell using fresh Coors Light beer as an electrolyte.

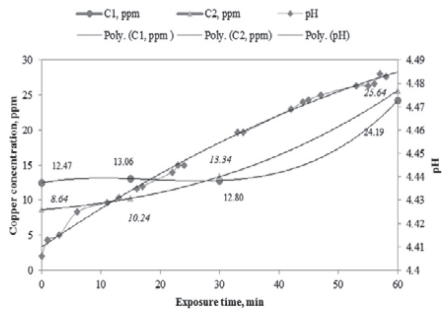

Fig. XI. Plot of copper concentration profiles (2 inputs) and pH as a function of exposure time in circulated electrochemical cell using mixed electrolyte from fresh Coors Light beer and Exp.2-used Coors Light beer electrolyte.

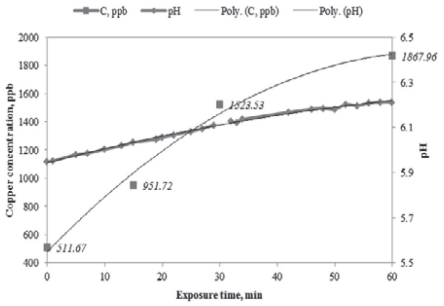

Fig. XII. Plot of copper concentration profile and pH as a function of exposure time in circulated-electrochemical cell using de-ionized water as an electrolyte.

B. Copper mass balance

From experimental runs # 2, 3, and 4, the copper weights corroded in an electrolyte in 60 minutes were calculated using Faraday's equation [5], as shown in Table II.

$W = MIt/nF$

W = the copper weight corroded in an electrolyte, g

t = exposure time = 60 × 60 s

M = atomic mass of copper = 63.546 g/mol

n = number of electrons produced or consumed in the process = 2

F = Faraday's constant = 96,500 C/mol or A.s/mol

I = cell current flow, A

Note: the accuracy of the current measurement was in the 2nd decimal.

In the electrochemical cell operation, the copper concentration was measured as a function of exposure time, 15, 30, and 60 min. The copper weights gained (Table III) in the electrolyte were calculated from the total electrochemical cell volume and the difference between the concentration input and output.

The data from Table II and Table III was used to calculate approximated weight gained and copper concentration, which were summarized as Table IV. The comparison of the theoretical and the experimental results between copper weight loss and weight gained was also shown in this Table.

TABLE II
CALCULATED ANODE WEIGHT LOSS IN AN ELECTROLYTE IN 1 HOUR.

Operating conditions	**Exp. Run # 2** Static, fresh Coors Light beer	**Exp. Run # 3** Circulation, mixed fresh Coors Light beer and Exp.2-used electrolyte	**Exp. Run # 4** Circulation, de-ionized water
Cell current reading (I)	0.13 A	0.13 A	0.00 A
Anode weight loss (Table I)	**0.16 g**	**0.14 g**	**0.11 g**
Calculated anode weight loss *(W = MIt/nF)*	0.1541 g	0.1541 g	0.01 g (using max. value of 0.005 A)
Comparison of anode weights loss between the experimental and the calculated values by the deviation, Δ : Δ = (Exp. – Cal.) × 100 Exp.	+3.69 % deviation Look the same.	-10.07 % deviation • 10.07 % copper ions absence might cause precipitates of sulfides, oxides, and hydroxide.	+90.9 % deviation • The high weight loss came from the golden brown precipitate coated on anode surface area. • The low, 0.00 A-cell current, means that there are trace ions diffusing to the electrolyte.

TABLE III
CALCULATION OF COPPER WEIGHTS GAINED IN THE ELECTROLYTE

Exposure time, min	**Exp. Run # 2** Copper concentration, ppm	**Exp. Run # 3** Copper concentration, ppm	**Exp. Run # 4** Copper concentration, ppb
0	**0**	**12.47** **8.64**	**511.67**
15	2.45	13.06 10.24	951.72
30	4.39	12.80 13.34	1,523.53
60	**6.39**	**24.19** **25.64**	**1,867.96**
[1]15-min *circulation after current shut down*		*[1]15.48*	
[2]30-min *circulation after current shut down*		Note: Comparison between 2 test runs	*[2]1,156.26*
Output-Input (ppm, mg/L)	6.39-0 = 6.39	Run-1: 24.19-12.47 = **11.72** Run-2: 25.64-8.64 = **17.0**	1,867.96-511.67 = 1,356.29 ppb **= 1,3563 ppm**
Total volume (L)	10	12	12
Copper weight gained (g)	6.39 × 10 = 63.9 mg = 0.0639 g	Run-1: **11.72** × 12 = 140.64 mg = ***0.1406*** g Run-2: 17.0x12 = 204.0 mg = ***0.2040*** g	1.3563 × 12 = 16.2755 mg = 0.0163 g

Calculation of approximated weight gained
(Exp. Run # 2)

- The new output copper concentration from the input concentration of Run # 3 was estimated to be 12.47 ppm (Table III, [c] = 12.47 ppm at exposure time = 0 min).
- Approximated one third of fresh beer was mixed with approximated two third of Exp. Run # 2 electrolyte.

Therefore,

$$(1/3)(0 \text{ ppm}) + (2/3)(y \text{ ppm}) = (12.47 \text{ ppm})(1/3 + 2/3)$$
$$y = 12.47 \times (3/2) \text{ ppm}$$

Run # 2 estimated output concentration
= 18.705 ppm
Output – Input = 18.705 - 0 ppm
= 18.705 ppm
Weight gained in 10-l electrolyte
= (18.705 × 10)/1000 g
Approximated copper weight gained
in Run # 2 electrolyte = **0.1871** g

➢ The approximated copper weight gained of **0.1871** g was closer to the weight loss of 0.16 g and the calculated weight loss of 0.1541 g (Table II).

Calculation of copper concentration (Exp. Run # 3)

- Let the maximum copper anode dissolution was equal to 0.20 g/h (Maximum anode weight loss in Table I = 0.16 g/h).
- From the actual continuous beer flowrate of 4.75 L/s (1.25 gal/s), the concentration of copper in the beer stream was calculated as the following.

Copper concentration in 4.75 L/s-beer stream
= (0.20 × 1000 × 1000) / (4.75 × 3600) ppb
= 11.70 ppb

From the operating conditions of Exp. Run # 3, cell current reading after 60-min operation was 0.13A (Table I). *From the results of Exp.3 and Exp.4, cell current varied with the concentration of copper in the electrolyte.*

Assumed that 0.15 A was the maximum cell current reading.

If the current was set as 0.50 A, therefore the copper concentration
= (0.5/0.15) x 11.7 ppb or *39 ppb*.

It was in *the range of 30-50 ppb of expected copper concentration* in the beer stream.

TABLE IV
COMPARISON BETWEEN THE THEORETICAL AND EXPERIMENTAL RESULTS OF COPPER WEIGHTS

Operating conditions	**Exp. Run # 2** Static, fresh Coors Light beer	**Exp. Run # 3** Circulation, mixed fresh Coors Light beer and Exp.2-electrolyte	**Exp. Run # 4** Circulation, de-ionized water
Anode weight loss (Table II)	**0.16 g**	**0.14 g**	**0.11 g**
Calculated anode weight loss *(W = MIt/nF)* (Table II)	0.1541 g	0.1541 g	**0.01 g** (using max. value of 0.005 A)
Copper weight gained (g) (Table III)	6.39 × 10 = 63.9 mg = *0.0639 g*	11.72 × 12 = 140.64 mg = ***0.1406 g*** 17.0 × 12 = 204.0 mg = *0.2040 g*	1.3563 × 12 = 16.2755 mg = ***0.0163 g***
Results comparison and analysis	• The 60-min sample was not well-mixed because of the static condition. • Approximated copper weight gained from the *Exp. Run # 2 calculation* = ***0.1871 g***	• Copper gained was equivalent to copper loss • If let 0.20 g/h be the maximum copper anode weight loss, copper concentration from *Exp. Run # 3 calculation* = ***11.7 ppb*** in 4.75 L/s beer stream flowrate.	• Copper gained was equivalent to calculated copper loss • More weight loss came from the scrubbed golden brown compound on anode surface.
Current efficiency = actual copper loss or gained / theoretical copper loss or gained	= 0.16/0.1541 = 1.04 *100 % of the current was effective in anode reaction.*	= 0.14/0.1541 = 0.91 *91 % current efficiency on anode reaction.*	= 0.0163/0.01 = 1.63 *100 % current efficiency*

IV. THEORETICAL DISCUSSIONS

A. Electrochemical Reactions

Because of the low pH, the trace amount of H_2S can dissociate to sulfide ion.

$$H_2S = H^+ + HS^-$$
$$HS^- = H^+ + S^=$$

Anodic reaction;

$$Cu = Cu^{++} + 2\,e^-$$
$$Cu = Cu^+ + e^-$$

Cathodic reaction;

$$2H^+ + 2e^- = H_2$$
$$Cu + H_2S\,(aq) = CuS + H_2\,(g)$$
$$Cu + 2H_2S\,(aq) = CuS_2 + 2H_2\,(g)$$
$$2Cu + H_2S\,(aq) = Cu_2S + H_2\,(g)$$

The more copper ions dissolved from anode reaction, the more sulfide ions eliminated from H_2S to form copper sulfides. From the diagram in Fig. XIII [6], the more HS- produced, the less H_2S in the beer stream. The reaction shifts to the right. As a result, H_2S is eliminated from the beer stream.

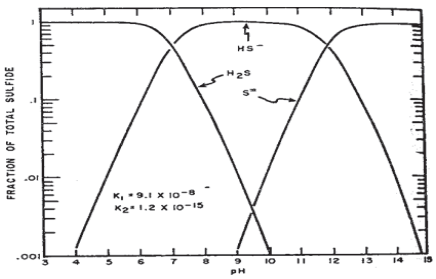

Fig. XIII. Approximate distributions of H_2S, HS^-, and S^-

Because pH of the Coors Light beer is lower than 7, at pH values of around 4-5, oxygen dissolved in the beer electrolyte performs the cathodic reaction.

$$O_2 + 4H+ + 4e- = 2\ H_2O$$

This reaction accepts electrons from anodic reaction and it causes higher rate of copper dissolution from anode. The protons from H_2S dissociation are supposed to be the small amount compared with the electrons from copper dissolution because of the trace amount of H_2S in the beer. As a result, it is possible that oxygen might have another cathodic reaction.

$$1/2\ O_2 + 2e^- = O_2$$

Therefore, except the sulfide compounds of copper, some oxides of iron and copper, i.e. CuO, Cu_2O, FeO, FeS, and Fe_2O_3, could be formed and deposited on cathode surface.

From the X-ray diffraction analysis results, the rust compounds fouling on cathode surface were Cu_2S, CuS_2, CuS, Cu, CuO, Cu_2O, Fe_2O_3, FeO, and FeS. Their formations are explained by these electrochemical reactions. The excess copper ion forms copper oxide with dissolved oxygen. Some accepts electrons from iron and causes copper metal deposit on cathode, too.

B. Electrode Fouling

Let 12 L-total volume of circulated-electrochemical cell and 1-h operation;

For minimum 50 ppb Cu/electrolyte,

copper weight = (50/1000) mg/L × 12 L
= 0.6 mg = 6×10^{-4} g
= 6×10^{-4} / 63.546
= *9.44×10^{-6} g-mole*

The sulfides of copper were supposed to be Cu_2S, CuS, or CuS_2. The maximum g-mole of H_2S needed is 2 g-moles per 1 g-mole of Cu for CuS_2. That is equal to $2 \times 9.44 \times 10^{-6} \times 34.064$ or 6.4313×10^{-4} g or ***53.59 ppb*** of H_2S in 12-L electrolyte volume.

The amount of sulfide precipitate gained depended on the trace concentration of H_2S or sulfur compound in the beer stream.

- Consider CuS, which consumed half of *53.59 ppb* or ***26.80 ppb*** of H_2S in 12-L electrolyte volume.
- *Assumed that the rate of copper ion eliminated was 9.44×10^{-6} g-mole/h.*

The rate of CuS produced
= 9.44×10^{-6} g-mole/h
= $9.44 \times (63.546 + 32.064) \times 10^{-6} \times 1000$ mg/h
= 0.9026 mg/h

For **120 hours of operating time**,

CuS produced = 0.9026×120 = 108.31 mg
= 108.31 mg / 150 cm^2 of cathode surface area
CuS density [2] = 4.6 g/cm^3
Then, CuS thickness
= $(108.31 \times 10^{-3}/4.6)\ cm^3/150\ cm^2$
= $(1.5697 \times 10^{-4}$ cm) × (10 mm/cm)
= **0.0016 mm**

The CuS calculated thickness on cathode surface was not high. However, the electrode fouling was caused from both sulfides and oxides.

Assumed that the maximum g-mole of the corrosion products occurred was approximately 100 times of CuS produced, therefore the scale thickness was approximately 0.16 mm or 0.2 mm.

[Cu] = 100 × 50 = 5,000 ppb (ppm)

Operating time of 120 hours was possible before electrode cleaning. However, the efficiency for the formation of oxides and sulfides of copper and iron was not 100%. That caused the amount of copper, which dissolved from anode, was higher than 50 ppb. If the rate of anode copper dissolution was equal to the rates of formation of the oxide and sulfide scale on cathode, the copper ions should not be detected from an electrolyte.

C. The relation between the electrode surface and the cell current

For the copper electrodes in the electrolyte, the resistance of the electrolyte is defined as [7, 8]:

$$R = \frac{v}{I} \quad \text{(Ohm's law)} \quad \ldots\ldots\ldots\ldots(1)$$

$$R = \frac{1}{\kappa} \cdot \frac{L}{A} \quad \ldots\ldots\ldots\ldots(2)$$

Where,
V = Volts applied
I = Cell current reading, amperes
L = Average length of flow path or the distance gap between both electrodes, cm
A = Copper electrode cross-sectional area, cm^2
= Conductivity of the electrolyte, $ohm^{-1}cm^{-1}$
= $L\,c^*$ ……(3)

Where,
Λ = Equivalent conductivity, $ohm^{-1}cm^2eq^{-1}$
c^* = Copper concentration in the electrolyte, equivalents cm^{-3}

Let
x = g-moles or equivalents of copper dissolution to the electrolyte from anode
z = g-moles or equivalents of copper oxides and sulfides fouled on cathode surface
= x (if rate of anode copper dissolution is equal to cathode oxides and sulfides formation)
c = g-moles or equivalents of copper in the electrolyte
= x – z (If z = 0, c = x) ……(4)
y = g-moles or equivalents of theoretical copper dissolution

If ε = Cell current efficiency
= x / y ……(5)
v = Total volume of electrolyte in the electrochemical cell, cu cm

Then, $c^* = \frac{c}{v} = \frac{x - z}{I}$

$= \frac{\varepsilon y - z}{v}$ .....(6)

Combination of (1), (2), (3), and (6),

$$\frac{v}{I} = \frac{1}{\kappa} \cdot \frac{L}{A} = \frac{1}{\Lambda \cdot C^*} \cdot \frac{L}{A}$$

$$= \frac{1}{\Lambda \cdot (\varepsilon y - z) / v} \cdot \frac{L}{A}$$

$$= \frac{v}{\Lambda \cdot (\varepsilon y - z)} \cdot \frac{L}{A}$$

$$(\varepsilon y - z) = \frac{v}{\Lambda} \cdot \frac{L}{A} \cdot \frac{I}{v}$$

$$z = \varepsilon y - I \left(\frac{v}{\Lambda} \cdot \frac{L}{A} \cdot \frac{1}{v} \right) \quad \text{.....(7.1)}$$

or

$$z = x - 1 \left(\frac{v}{\Lambda} \cdot \frac{L}{A} \cdot \frac{1}{v} \right) \quad \text{.....(7.2)}$$

or

$$c = I \left(\frac{v}{\Lambda} \cdot \frac{L}{A} \cdot \frac{1}{v} \right) \quad \text{.....(7.2)}$$

The distance gap (L), the electrolyte volume (v), the voltage applied (V), and the electrode surface area (A) are known. The cell current reading (I) and the copper concentration in the beer electrolyte (c) can be measured from the experiment runs. The equivalent conductivity (Λ) at each copper concentration in the beer electrolyte can be calculated from equation (7.3).

From the correlations of Eq. 6 and Eq. 7.3, the equivalent conductivity depends on the ion concentration in the electrolyte. The higher the concentration, the lower the equivalent conductivity.

Note: Some experiments might be performed to investigate the correlation between the equivalent conductivity and the copper ion concentration in the beer stream. The expected equivalent conductivity is supposed to input in equation (7.1) or (7.2) to calculate "z" or g-moles of oxides or sulfides of copper fouled on cathode surface.

Consider the voltage applied and the cell current reading (Eq. 4 and Eq. 7.3),

$$c = I \left(\frac{v}{\Lambda} \cdot \frac{L}{A} \cdot \frac{1}{v} \right) = \frac{I}{v} \left(\frac{v}{\Lambda} \cdot \frac{L}{A} \right)$$

or $c = x - z = \frac{I}{v} \left(\frac{v}{\Lambda} \cdot \frac{L}{A} \right)$

$$= \frac{1}{R} \left(\frac{v}{\Lambda} \cdot \frac{L}{A} \right)$$

The relations can be compared as the diagram in Fig. XIV.

The fouling (z) will be reduced with the reduced voltage (V) applied. The lower electrolyte resistance (R) will increase the cell ampere reading (I) and that causes more copper ions (c) in the beer electrolyte.

By conclusion, to reduce the copper ion concentration in the beer electrolyte means the fouling scale increases with the decreasing of the cell current. The voltage applied should be higher.

Fig. XIV. Comparison between various critical functions.

V. Conclusions

This corrosion research program was performed in 2000-2001 at Corrosion Laboratory, MME Department, CSM, CO, USA, under the sponsorship of Coors Brewing Co.

Two electrolytes, water and beer, were provided by this Brewing Company. The data obtained was compared with the actual plant parameters of 25 V and 1.4 A on an anode surface area of 260 cm^2. This Coors process, of year 2000-2001, was operated at 5-6 A/cm^2 at applied voltage of 25 V. The actual continuous beer flow rate was 4.75 L/s (1.25 gal/s). The electrode gap of old prototype was ¾-in but it was modified to 1.5-in for the new prototype.

Two factors were departure from the actual process, which maintained 1.25 gal/s continuous high beer electrolyte flow rate. Both were; 1) The sulfide ion-bearing electrolyte was not applied to the simulated process; and 2) The flow condition of the electrolyte was restricted to the recirculation type only.

The effects of the electrode separation and the electrode surface area on the efficiency of copper dosing of the beer stream were evaluated from the experimental results.

Following conclusions were drawn from this work:

a) Under static condition at room temperature;

• The process was current limited at 0.5 A in the cell configuration used. This limiting current increased with flow of electrolyte and temperature (Fig. II).

• Local buildup of copper ions along the anode surface caused the precipitation of copper hydroxide at higher voltages as well as higher current density, i.e. fast rate of copper ion formation (Fig. II).

b) Under circulated condition at room temperature;

• The amount of copper ions added to the homogeneous recirculated beer, at a maximum process current of 0.15 A and 150 cm^2 anode areas, was 11-12 ppb per second. This was equivalent to 0.15-0.20 g of copper in one hour (Fig. XI).

• In a flowing system, no buildup of local copper ion concentration to cause copper hydroxide precipitation.

c) Other investigation results;

• Under identical conditions of electrode separation, surface area and cell voltage, higher current was

preferred to achieve in the beer than in the water due to higher electrical conductivity and lower pH of the electrolyte (Fig. VII, VIII, and IX).

• The 60-min duration experiments illustrated that over 95% current efficiency, the copper material balance was matched by anode weight loss and electrolyte ion concentration (Table I, II, and III)

• At the calculated rate of copper dosing to the stream, no cathodic deposition of copper was expected. Formation of copper sulfide was a highly preferred reaction over copper hydroxide precipitation and sulfide formation was the most desired reaction for copper ions in the system (Electrochemical reactions discussion).

• Electrode fouling was caused from both sulfides and oxides. [Cu] or "c" decreased with decreasing cell current (I) and increasing voltage (V), which caused increasing of fouling scale (z) (Fig. XIV).

d) Recommendations;

• For the same electrode separation, the current density (I/A_E) change was higher with the lower surface areas (A_E), as in Fig. IV. From Ohm's law, R = V/I, the increasing of the current (I) and I/A_E effects the decreasing of cell resistance (R). Therefore, it was supposed to lower the anode surface areas.

• The voltage (V) should be adjusted to achieve the desired current (I), as well as lowering by decreasing the cell resistance (R), as illustrated in Fig. XIV.

• Electrode gap of ¾-in to 1-in was optimum for high current efficiency (Fig. V). If possible, the electrode gap should be maintained at ¾-in.

• Good electrolyte-electrode contact was desired in the flowing system to add the copper ions doses effectively for sulfur capture.

• The electrode surface area should be adjusted to achieve a minimum current of 0.5 A. At this current the copper dose was in the range of 35-40 ppb (Exp. Run # 3 Calculation of copper concentration). This range was the limited [Cu] in the beer stream for removing trace H_2S and other sulfur compounds.

Acknowledgements

The author would like to express the sincere gratitude to my Ph.D. Advisor (2000-2002), Dr. Brajendra Mishra, Research Professor of Department of Metallurgical and Materials Engineering, Colorado School of Mines (CSM), CO, USA, for his guidance, concepts, advices, and support. Thanks for some MME laboratories that allowed me to use their weight balances, as well as the support from MME Machine shop for some mechanical work. Some helpful advices from another MME graduated students about the instruments and equipment were also recognized.

Thanks for the permission and cooperation of CSM Physics Department for the author to operate their X-ray diffraction analyzer. The deionized water, some glassware, and some chemicals from CSM Chemical Store of Chemistry Department were also thankful.

The cooperation of Regulatory Technical Support Division for my article presentation in this Technical Conference is also appreciated.

References

[1] A.T. Kuhn, *Industrial Electrochemical Processes*, Elsevier Publishing Co., New York, NY, 1971, pp 226-230.

[2] Perry & Green, *Perry's Chemical Engineers' Handbook*, 6th ed., McGraw-Hill Book Co., New York, NY, 1984, pp 3-12 - 3-13.

[3] Geoffrey Prentice, *Electrochemical Engineering Principles*, Prentice Hall, New York, NY, 1991, pp 32.

[4] L.B. Pankratz et al., *Thermodynamic Data for Mineral Technology*, Bulletin 677, United states Department of Interior Bureau of Mines, 1984.

[5] William F. Smith, *Foundations of Materials Science and Engineering*, 2nd ed., McGraw-Hill Book Co., New York, NY, 1993, pp 663-671.

[6] Kane, R.D., Roles of H_2S in behavior of engineering alloys, *International Metals Review*, vol. 30, no. 6, 1985, pp 291-301.

[7] Owen F. Devereux, *Topics in Metallurgical Thermodynamics*, Krieger Publishing Co., Malabur, FL, 1983, pp 180-183.

[8] Robert D. Pehlke, *Unit Processes of Extractive Metallurgy,* 2nd ed., American Elsevier Publishing Co. Inc., New York, NY, 1975, pp 201-225.

Jarunee Kraikaew was born in Nakhonsrithammarat province, on November 03, 1957. She received BSc. (Chemistry) in 1978 from Kasetsart Unversity, and MSc. (Chemical Technology, Major Chemical Engineering) in 1983 from Chulalongkorn University, in Bangkok, Thailand. In 1998, she received another MSc. (Metallurgical and Materials Engineering) from Colorado School of Mines, Colorado, USA.

She started working with Office of Atomic Energy for Peace (OAEP) from Jan. 15, 1979, as a Nuclear Chemist, Level 3, in Nuclear Raw Materials Development Project, Chemistry Division. Her present position in 2017 is Senior Professional Nuclear Chemist, Level 8, in Regulatory Technical Support Division. From 1979 to 2007, she worked as a researcher in this said project to develop some process equipment design and control in monazite processing semi-pilot plant and had some researches in U-Th-RE separation and purification. She has around 38 published research papers in domestic and international Journals and Conferences, and OAEP (OAP) annual reports / technical reports at that time.

From 1992-present, she has more experience in Nuclear technology and engineering, especially NPP and NKM, from some domestic/international seminars, training courses, workshops, conferences, and IAEA E-Learning. In year 2007-2014, she has around

25 articles in nuclear and radiation in OAP Nuclear Review, Thai Nuclear Society website, and NST-2011 Conference. She also had wnn.com-nuclear news translation, E-books, booklets, and NPP database distribute in public domain, as OAP website and free CD copies for concerning organizations and public. From 2014-present, she had an opportunity to go oversea to attend international Conferences in Nuclear Fuel Cycle and Research Reactor, as well as participating in three international TC /WS in nuclear material(NM) regulatory and physical protection. At present, she earns more publications, i.e. 2 on-line published articles in International Journal/Conference, 2 unpublished technical English reports from these TC /WS, and 3 unpublished technical translation books. In 2016, she succeeded in developing NM database via Microsoft Access-2010 and creation of CourseLab module and multimedia demonstration. At present, except technical translation concerning with National Nuclear Forensic Library (NNFL), she is setting up special nuclear material database, which is expected to support the development of OAP-NNFL in the future.

Ms. Jarunee Kraikaew is the membership of 1) National Research Council of Thailand; 2) Thailand Council of Engineers; 3) Nuclear Society of Thailand; and 4) National Metal and Materials Technology Center (02/2004-02/2005). On Mar. 31, -Apr. 01, 2006, She had Thai oral presentation on "Solvent extraction study of rare earths from nitrate medium by the mixtures of TBP and D2EHPA in kerosene", in The Fourth Thailand Science and Technology Conference. She was honored two awards, "Best Paper Award in Metals and Manufacturing and Design Session" from this Conference and "Best Paper Presentation Award in Metal Session" from Iron and Steel Institute of Thailand.

Brajendra Mishra received his Bachelor of Technology [1981] in Metallurgical Engineering from the Indian Institute of Technology in Kharagpur, India. He earned M.S. [1983] and Ph.D. [1986] in Materials Science from the University of Minnesota in Minneapolis.

He is a Colorado School of Mines (CSM) research professor and used to be associate director of Kroll Institute for Extractive Metallurgy and Advanced Coatings & Surface Engineering Laboratory at the CSM. Prior to joining CSM in 1990, Prof. Mishra served at Tata Steel in India. He has also served as a Faculty Consultant for Motorola Corp. Prof. Mishra is the President of faculty Senate [2006-08] at CSM.

Dr. Mishra's current research interests and contributions are spread over two major needs of the day - Environmental management by developing chemically benign processes and - Materials development with enhanced properties. His research interests bridge across the process and the physical metallurgy of materials. He is the author of more than 600 publications, including more than 280 papers in peer-reviewed journals. He has also edited 18 books and written seven chapters on chemical processing and extractive metallurgy.

He served as a trustee of the American Institute of Mining, Metallurgical and Petroleum Engineers (AIME) from 2007 to 2012 and its president in 2011. He was president of TMS (the Minerals, Metals and Materials Society) in 2006. His scholarship and leadership has been honored with a number of awards, including Honorary Membership, the highest award bestowed by the Indian Institute of Metals; the Alexander Scott Distinguished Service Award from TMS; Honorary Professor of Kazakh National Technical University and the Presidential Citation from AIME.

Sources: 1) http://metallurgy.mines.edu
2) http://www.aimehq.org/about-us/people/past-trustee/brajendra-mishra

Modeling the Dynamic Individual Activity Decision Behavior Through the Influence Diagram Model

Natachai Wongchavalidkul

The Cluster of Logistics and Rail Engineering, Faculty of Engineering, Mahidol University, Salaya, Phuttamonthon, Nakhon Pathom, Thailand
E-mail: natachai.won@mahidol.ac.th

***Abstract*—Using the Influence Diagram (IFD), this paper attempted to model the human decision behaviors on choosing their daily activities by considering both the features of human decisions and the expected utilities outcomes of decisions. The 2004 time use survey data from the National Statistical Office (NSO) which represents 2,573 individuals in Bangkok were utilized as the case study in the paper. As the results, there are 19 proposed IFD models based on types of populations and number of members in the household. Results from the model validation processes also presented that all 19 IFD models were successfully simulated the activities (ACT) and the decisions of whom in the household to do activities with (WHO). The IFD model is expected to be better represent individual activity decisions than the Classification and Regression Tree (CART) model and the Bayesian network model as its incorporated the utility scores in the decision processes.**

***Index Terms*—Influence Diagram Model, Classification and Regression Tree, Particle Swarm Optimization, Activity Decision Behavior.**

I. Introduction

Individual and family traveling behavior has been incorporated into transportation traveling demand model in several ways. Models are differently considered person traveling behavior based on either the modeling structure and framework or the data availability. In general, the traditional traveling demand model represents persons' traveling behavior in the part of the modal split and the traffic assignment. However, the model still represents the demand of persons in the aggregate level of geography, known as Traffic Analysis Zone (TAZ).

The new concepts of travel demand modeling are interested in more details of person decisions and their traveling behavior. Several types of models have been introduced among these models. The activity based travel demand model catches up both researchers and practitioners in the field. However, based on its details and complexities, further researches are needed in order to solve several limitations in its concepts.

The activity based travel demand model is one of the most complex travel demand models that are trying to analyze the travel demand based on the individual activities behavior. In brief, the model is disaggregating analyze the individual persons in the study area (rather than concentrating on the zonal behavior, TAZ). Hence, several models are required to apply in this concept from generating locations of individual in the study area, analyzing their activity patterns, to estimating their traveling route decisions. This paper concentrates on the problem of modeling individual activity patterns based on their dynamic decisions.

Human decisions are uncertainty and consequences. Decisions are made under circumstances and those with the highly familiar are usually selected. Beside, time is also the important factor affected to the decisions. Decisions could be made over times, at one single time step, or under the time constraint. Human are normally making decisions by considering these tree features: the uncertainty, familiarity and expertise, and time [2]. On the other hand, Russell and Norvig restated the written of French philosopher Arnauld, written in 1662, regarding to the logic of human decisions as follows [5].

"To judge what one must do to obtain a good or avoid an evil, it is necessary to consider not only the good and the evil in itself, but also the probability that it happens or does not happen; and to view geometrically the proportion that all these things have together."

The good and evil in the context can be considered as the utility. The utility is a single number that expresses the desirability of a state. In the other word, human preferences between choices can be captured by utilities. In general, each decision choices are uncertainty. Hence, the combination of utilities (preferences) and probabilities (uncertainty) of choice decisions is the expected utility. In summary, human are making their decision based on their familiarity and expertise, time, and the expected utility.

The prior discussions of human behavior are considered to be true for the daily activity decision

behavior. Using the Influence Diagram (IFD), the purposed model in this paper attempted to follow the prior assumptions on human decision behaviors by considering both the features of human decisions (the uncertainty, familiarity and expertise, and time) and the expected utilities outcomes of decisions.

II. Theoretical Background

A. The Influence Diagram (IFD)

The influence diagram (IFD) is a Bayesian network with integrations of action nodes and utility nodes. It is a directed acyclic graph with three types of nodes including the decision node, the chance or probabilistic node, and the utility node. The decision node represents the decision variables (choices of actions). The chance node represents random variables. These variables are the same as those used in the Bayesian network. Finally, the utility node describes the utility value (function) of its parent node [5]. Additionally, in this study, the discrete IFD is proposed. A discrete influence diagram (N) = (X, G, P, U) consists of:

- a Direct Acyclic Graph (DAG) (G) with nodes (V) and directed link (E)
- a set of discrete random variables (XC) and discrete decision variables (XD) such that X is a set of XC and XD, represented by nodes of G
- a set of conditional probability distributions (P) or conditional distribution table (CPT) containing one distribution $P(X_v | X_{pa(v)})$, for each discrete random variables Xv
- A set of utility function, U, containing one utility function, u(Xpa(w)) for each node w in the subset $V_u \subset V$ of utility nodes [6]

Given the structure of the IFD as prior discussions, the set of expected utility (EU) can be computed from the diagram as the following equation, (1).

$$EU(X) = \prod_{X_v \in X_c} P(X_v | X_{pa(v)}) \sum_{w \in V_u} u(X_{pa(w)}) \quad (1)$$

In general, the alternative (a^*) which has the highest expected utility is proposed as the decision alternative. It is also known as the maximum expected utility principal, as stated in equation (2).

$$a^* = \arg\max EU(X) \quad (2)$$

However, in order to apply results of the expected utility to the individual decision behavior, the maximum expected utility principal is relaxed. Instead of selecting the activity which has the maximum expected utility, the model randomly selects the activity which probability is based on the value of expected utility, as shown in equation (3). Hence, the model will be more flexible on the decisions rather than only restricting decisions to the maximum expected utility.

$$a^* \sim EU(X) \quad (3)$$

B. Particle Swarm Optimization (PSO)

Briefly, PSO is a population based stochastic optimization technique. Two specific inspiration of the algorithm are fish schools and bird flocks. These natural behaviors represent the collections of particles (elements) that synchronously move together. The particles are moving together, diverging from another, and then regrouping in order to find the best solution. The algorithm works in two main steps, calculating the particle velocity and updating particle position. In the other words, the particles are recalculated its velocities and decide whether to move to the new position or not. Also, the moving decision will be made only the new position is gained the particle's values. Applications of PSO algorithms can be found in Pulido and Coello [3] and El-Zeonkolv [1]. The main properties of the PSO algorithms using in this study can be summarized as follows.

- The position of each particle is the utility values of a given ACT and WHO, u(ACT, WHO). The u(ACT, WHO) positions were also constrained as its coordinate values must be between 0 and 1 and the sum of the coordination values in each particle must be equal to 1.
- The score function of each particle is the Chi-square value gathering from the Chi-square test between the set of generated activities from the model at the given particle's position, u(ACT, WHO), and the target activities from the training data. Further, there are two scoring values to track. First, the P_{best} value is the best score that each particle can be gathered. Second, the G_{best} value is the score of the particle that have the best (minimum) score comparing to other particles in the swarm.

The velocity of each particle is calculated based on the particle's current position and the position of the G_{best} particle. Equation (4) presents the velocity calculation using in this research.

$$V_{k+1} = w \times V_k + r_1 \times (POS\_P_{best,k} - x_k) + r_2 \times (POS\_G_{best,k} - x_k) \quad (4)$$

Where:

- V_k is the current velocity of the particle, iteration k
- r_1 and r_2 is random numbers between 0.1 and 0.2 [3]
- w is the inertia weight, which this research took a value randomly generated within the range [0.1,0.9] [3]
- POS_P_{best} is the particle's position which has the best score (P_{best})
- POS_G_{best} is the position of the particle's which has the best score in the swarm (G_{best}).
- x_k is the expected new particle position, $x_k = x_{k-1} + V_{k-1}$

The perturbing function is used to perturb the swarm at the beginning period of the iterations. The main objective is to avoid the problems of particles' trapping in the local optima. Recommended by Pulido and Coello [3], equation (5) presents the perturb

function used in this research. Further, in this research the perturbed particle will randomly jump to the new position which is assigned by equation (6).

$$Prob_{turbulence} = (\frac{N_{iter}}{Total_{iter}})^{1.7} - 2.0 \times (\frac{N_{iter}}{Total_{iter}}) + 1.0 \quad (5)$$

Where:
- $Prob_{turbulence}$ is the probability of the perturbed action
- N_{iter} is the number of the current iteration
- $Total_{iter}$ is the total number of the iterations

$$X_{perturb} = 2 \times RandomNumber \times X_k \quad (6)$$

Where:
- $x_{perturb}$ is the new position of the perturbed particle.
- x_k is the expected new particle position, $X_k = X_{k-1} + V_{k-1}$

- The stopping criteria assigned in this study is the total number of iterations. The total number of iterations was assigned by trials and errors (1,000 iterations were assigned in this study) to ensure that the G_{best} value given by the swarm was steady, no sign of the improvement.

Further, the problem can also be formulated in a form of the nonlinear programming problem as follows.

$$U_{jk} = \arg\max \left[\sum_{k=1}^{2} \sum_{j=1}^{37} \left(\frac{\left(N_{jk}^S - E_{jk}^S\right)^2}{E_{jk}^S} \right) + \sum_{k=1}^{2} \sum_{j=1}^{37} \left(\frac{\left(N_{jk}^T - E_{jk}^T\right)^2}{E_{jk}^T} \right) \right] (7)$$

Subject to:

$$0 < U_{jk} \leq 1\mathrm{U}$$

$$\sum_{k=1}^{2} \sum_{j=1}^{37} U_{jk} = 1$$

Where:
j = variable indicate type of activities (1-37), ACT
k = variable indicate if the activity involve with persons in the household or not (1-2), WHO
U_{jk} is the utility values of the given variables, j and k

$E_{jk}^S = \left(\frac{N_{jk} \times S}{N} \right)$ is the expected frequency of the simulated population in category j and k

$E_{jk}^T = \left(\frac{N_{jk} \times T}{N} \right)$ is the expected frequency of the target population in category j and k

$N_{jk} = N_{jk}^S + N_{jk}^T$ is the total number of simulated population and target population by category j and k

N_{jk}^S is the total number of simulated population by category j and k

N_{jk}^T is the total number of target population by category j and k

$S = \sum_{k=1}^{2} \sum_{j=1}^{37} N_{jk}^S$ is the total simulated population

$T = \sum_{k=1}^{2} \sum_{j=1}^{37} N_{jk}^T$ is the total target population

$N = S + T$ is the total simulated population and target population

III. Methodology

A. DATA FOR MODEL DEVELOPMENT

The 2004 time use survey data from the National Statistical Office (NSO) were utilized in this research. The data were sampled from different parts of Thailand, including Bangkok metropolitan area, central region, northern region, north eastern region, and southern region. In this research, Bangkok time use data was utilized. Daily activity schedule of 2,573 individuals from 1,013 households were recorded in the dataset. Additionally, 15 percent are single person households; 37 percent are two person households; 23 percent are three person households; and 25 percent are more than three person households. The data also includes both population socio-demographic attributes and daily activity attributes

B. THE PROPOSED IFD MODEL

Figure 1 presents the proposed IFD for the individual activity decision. The structure of the model is similar to the Bayesian network's structure, except that the IFD was introduced both decision nodes and a utility node into its structure.

Additionally, Table I - Table III describe definitions of each variable.

For this research, the nodes named as ACT and WHO were introduced as the decision node and the utility node was introduced into the model. The structure was simple constructed to the concept that the Activity (ACT) and the involvement of persons in the household in those activities (WHO) are depended to both the socio-demographic variables (i.e. number of member in the household, relationship of the person in the household, gender, age, and educational level, etc.) and the activity schedule variables (i.e. times of the day, activity time durations, and types of activities, etc.). Also, the relation between ACT and WHO will affect to the individual utility during the day as well.

Furthermore, the node "TYPE" in this model is the Type of persons which were classified and grouped using Classification and Regression Tree Algorithms. The processes of grouping and classifying persons based on their activity patterns are out of the scope of this paper but readers who interest can see more details in N.Wongchavalidkul and M. Piantanakulchai [4].

Additionally, equation (7) presents the mathematical formula of the proposed IFD structure (Fig. I.). The equation is derived from the general formula presented in equation (1). Further, the proposed IFD is the discrete IFD which is only comprised of the discrete node type. Therefore, the continuous variables, such as TDU and AGE (Table II) are discretized.

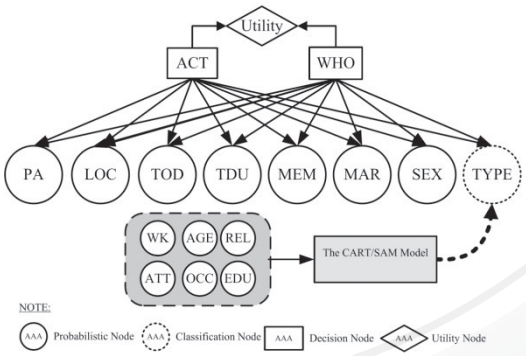

Fig. I. the Proposed IFD for Individual Activity Decision Behavior

$$EU(act, who \mid pa, loc, tod, tdu, mem, mar, sex, type) = P(pa \mid act, who)P(loc|act, who) P(tod \mid act, who)P(tdu|act, who)P(mem \mid act, who) P(mar \mid act, who)P(sex \mid act, who)P(type \mid act, who)u(act, who) \quad (8)$$

Given:

$act \in ACT, who \in WHO, pa \in PA, loc \in LOC, tod \in TOD, tdu \in TDU, mem \in MEM, mar \in MAR, sex \in SEX, type \in TYPE$

$X_D = \{ACT, WHO\}$ = *Decision Node*

$X_C = \{PA, LOC, TOD, TDU, MEM, MAR, SEX, TYPE\}$ = *Chance or Probabilistic Node*

$u(ACT, WHO)$ = *the utility of doing activity* (ACT) *with whom in the household* (WHO)

TABLE I
POPULATION SOCIO-DEMOGRAPHIC ATTRIBUTES

Variables	Description
PID	Personal ID (References for Survey Database)
MEM	Number of household members (age 10 years and over)
REL	Relationship of person in the household: 1. Householder, 2. Wife/Husband, 3. Single Son/Daughter, 4. Married Son/Daughter, 5. Son-in-law/Daughter-in-law, 6. Son/ Daughter's children, 7. Father/Mother/ Grandfather/Grandmother, 8. Relatives 9. Lodger or Servant
SEX	Gender: 1. Male, 2. Female
AGE	Age: 10-98 years old

TABLE I
POPULATION SOCIO-DEMOGRAPHIC ATTRIBUTES

Variables	Description
MAR	Marital status: 1. Single 2. Married
ATT	School Attendance: 1. Attending School 2. Not Attending School
EDU	Education: 1. Illiterate, 2. Less than Lower Elementary, 3. Elementary Level, 4. Lower Secondary Level, 5. Upper Secondary Level (General Programs), 6. Upper Secondary Level (Vocational Programs), 7. Upper Secondary Level (Educational Programs), 8. Diploma Level (Academic Programs), 9. Diploma Level (Technical Vocational Programs), 10. Diploma Level (Vocational Programs), 11. University (Academic Programs), 12. University (Technical Vocational Program), 13. University (Educational Lines), 14. Others, 15. Unknown
WK	Working status: 1. Employed, 2. Unemployed, 3. Wait for Working Season (Mainly Agriculture), 4.Housekeeper, 5. Study, 6. Children/Elderly, 7. Illness or Disabled, 8. Vacation/Retirement, 9. Others, 10. Age less than 15 years old.
RG	Religion: 1. Buddhism, 2. Christianity, 3. Islam, 4. Others
OCC	Occupation: 1. Employers, 2. Business Owner with no Employees, 3. Working for Family Business (No Salary), 4. Government Employee, 5. State Enterprise Employee, 6. Private Firm Employee, 7. Group / Organization, 8. Others

TABLE II
ACTIVITY SCHEDULE ATTRIBUTES

Variables	Description
TOD	Time of the Day (1-24)
TDU	Activity Time Durations (1-144, 10 minutes per step)
WHO	The person is doing the activity with members in the household or not (1. No, 2.Yes)
ACT PA LOC	Activity Code: 1-37 (see table 5.3 for details) the previous activity: 1-37 (see table 5.3 for details) Activity locations: 1-9 (1.Home, 2. Home of Others, 3. Work Places, 4. Public Places, 5. Shop/Entertainment Venue, 6. Schools/Collages/Universities, 7. Cultural or Sport Places, 8.Vehicles, 9. Others)

TABLE III
ACTIVITY CODES (ACT) FOR MODEL DEVELOPMENT

Code	Description	Code	Description
1	Working in private firm, government, state enterprise, or organizations	21	Reading books
2	Lunch break	22	Reading Newspaper / Magazine
3	Traveling for activity type 1 and 2	23	Watching television
4	Working others (Business owners)	24	Listening to the radio
5	Traveling for activity type 4	25	Surfing internet
6	Cooking	26	Using library
7	Cleaning and Housekeeping	27	Traveling for activity type 19-26
8	Laundry	28	Sleep
9	Shopping	29	Taking nap
10	Taking care of household members and pets	30	Eating snack
11	Traveling for activity type 6-10	31	Social drinking
12	Conversation / Phone conversation	32	Self care
13	Community services and socialization	33	Chant
14	Traveling for activity type 13	34	Conversation and talk with family members (family times)
15	Study in school system	35	Do noting / Relax
16	Homework /review lectures / tutorial classes	36	Reflective thinking and planning
17	Self study / part-time courses	37	Traveling for activity type 28-36
18	Traveling for activity type 15-17		
19	Playing games (arcades, computers, etc.)		
20	Jogging / exercises		

Note: highlighted cells are the traveling activities

C. MODEL BUILDING AND CALIBRATION

Two main processes were taken for the influence diagram model developments, the model building and calibration process and the model validation process. The input data were divided into two dataset. Ninety percent of the survey data were randomly selected and used as the training or calibrating data. On the other hand, the other ten percent were later used as the testing or validating data. Fig. II presents the model development processes for the influence diagram model developed in this research.

The additional steps are the construction of the influence diagram structure and the calibration of the utility values. From equation (3), there are two types of parameters needed to be estimated in the model. The first parameter is the conditional probability distribution. The second parameter is the utility values. The conditional probability distribution (P), P(XC|XD), for each variable can be directly estimated from the training data using the message passing in a tree junction method.

However, the utility function, u(ACT, WHO), or the utility values of given ACT and WHO variables, cannot be interpreted directly from the training data. In this case, the Particle Swarm Optimization (PSO) method was applied to find the best utility values of the proposed influence diagram. The PSO method was selected over the other method because it is well known and the method has been successfully applied in many researches and applications. The method also proved that it gets results in a faster, cheaper way compared to other methods such as the genetic algorithm. Additionally, PSO is attractive because it only requires very few parameters to adjust. Hence, it is very simple to apply the method to study problems.

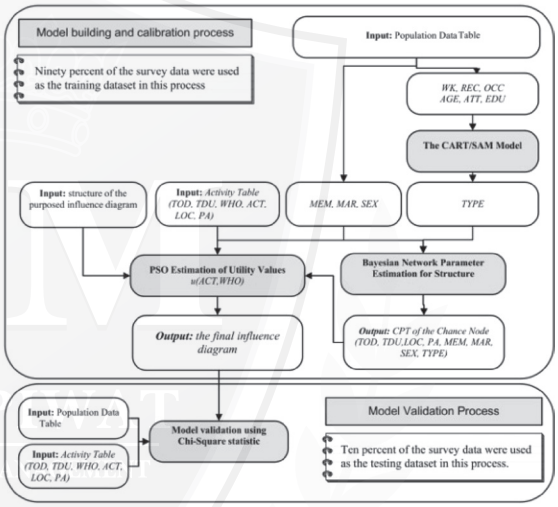

Fig. II. The IFD Model Development Processes

D. MODEL VALIDATION

The completed influence diagram developed in the previous section was then validated to qualify its ability in generating activity schedule. As mentioned in the previous section, the testing dataset was used in order to test performances of the model. In this research, the Chi-Square test was applied to compare the target activities in the testing dataset and the generated activities from the model. For the Chi-Square test, this research assumes that the P-value must be greater than 0.05 in order to accept the null hypothesis (Ho). The followings summarize the hypothesis testing used in the research.

Ho: *The distribution of the target populations and the simulated populations are not different*

$$\chi^2 = \sum_{k=1}^{2}\sum_{j=1}^{37}\left(\frac{\left(N_{jk}^{S}-E_{jk}^{S}\right)^2}{E_{jk}^{S}}\right)+\sum_{k=1}^{2}\sum_{j=1}^{37}\left(\frac{\left(N_{jk}^{T}-E_{jk}^{T}\right)^2}{E_{jk}^{T}}\right) \quad (9)$$

Note: Degree of freedom (df) = (r-1)(c-1) , df in this study = (72-1)(2-1) = 71

Where:

$E_{jk}^{S} = \left(\frac{N_{jk} \times S}{N} \right)$ is the expected frequency of the simulated population in category j and k

$E_{jk}^{T} = \left(\frac{N_{jk} \times T}{N} \right)$ is the expected frequency of the target population in category j and k

$N_{jk} = N_{jk}^{S} + N_{jk}^{T}$ is the total number of simulated population and target population by category j and k

N_{jk}^{S} is the total number of simulated population by category j and k

N_{jk}^{T} is the total number of target population by category *j* and *k*

$S = \sum_{k}^{2} \sum_{j}^{37} N_{jk}^{S}$ is the total simulated population

$T = \sum_{k}^{2} \sum_{j}^{37} N_{jk}^{T}$ is the total target population

$N = S + T$ is the total simulated population and target population

IV. Results of Model Development

From results of the calibration and validation process, it was found that the utility values calibrated from the proposed model structure in Fig. I. did not pass the validation process (P-value < 0.05). The reasons would be that the estimated utility values in the model were too general and could not be represented all types of persons in the model. In other words, the utility values are expected to be different from one type of persons to the others. Hence, the models were divided by types of population and individually calibrated for each type. Fig. III. presents the model structures for each population type. On the other hand, in order to pass the validation process, model for population type 7 was also divided by the variable indicated number of household members (MEM). Three categories of the variable MEM specified in the model of population type 7 are a single household (MEM = 1), a household with two members (MEM = 2), a household with three members (MEM = 3), and a household which has more than three members (MEM > 3).

Further, Fig. IV. presents the calibration results of the models for population type 1-9 (employment) and Fig. V. presents the calibration results of the models for population type 10-16 (unemployment). Table IV. summarized the final influence diagram developed in this research as well as the results from model validations.

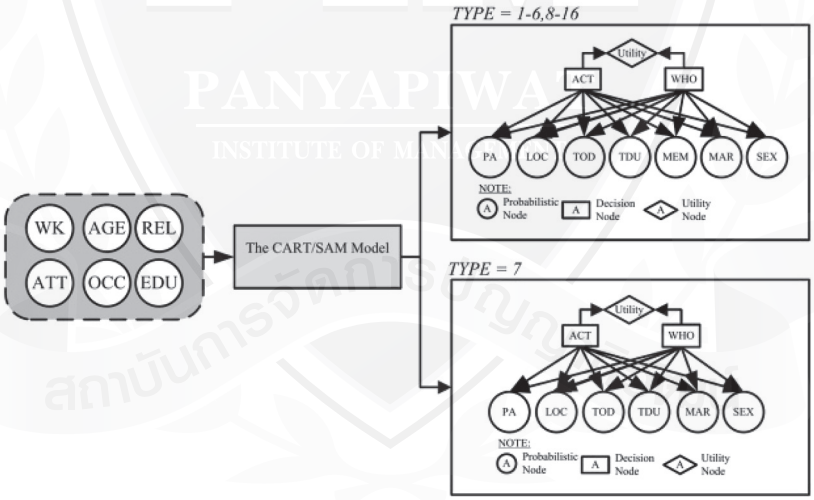

Fig. III. Final influence diagram structures

Note: for population type 7, the models were separately calibrated by variable MEM = 1, 2, 3, and more than 3

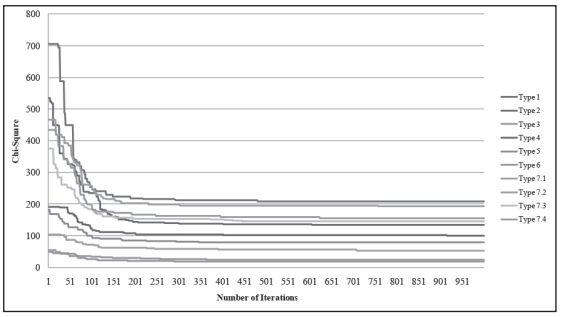

Fig. VI. Calibration Results of the Models for Population Type 1-9 (employed)

Note: type 7.1 (TYPE 7, MEM=1), type 7.2 (TYPE 7, MEM=2), type 7.3 (TYPE 7, MEM=3), type 7.4 (TYPE 7, MEM= more than 3)

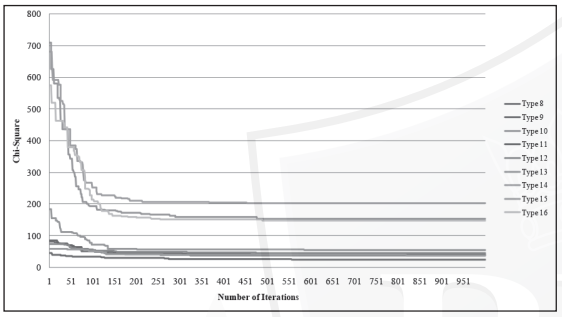

Fig. V. Calibration Results of the Models for Population Type 10-16 (unemployed)

TABLE IV
SUMMARY OF THE FINAL INFLUENCE DIAGRAMS AND THEIR VALIDATION RESULTS

Model	Variable		Chi-Square	P-Value
	TYPE	MEM		
1	1		61.103	0.782
2	2		50.284	0.966
3	3		14.874	1.000
4	4		37.758	0.999
5	5		29.631	1.000
6	6		15.892	1.000
7.1	7	1	18.175	1.000
7.2	7	2	52.169	0.950
7.3	7	3	41.570	0.997
7.4	7	> 3	50.732	0.966
8	8		21.099	1.000
9	9		16.670	1.000
10	10		52.348	0.939
11	11		30.208	1.000
12	12		25.954	1.000
13	13		32.076	1.000
14	14		43.798	0.996
15	15		28.730	1.000
16	16		48.860	0.962

Note: P-value must be greater than 0.05 in order to pass the validation processes

V. SUMMARY AND DISCUSSIONS

The IFD model developed in this paper is targeted to model the decision behavior of the individual persons. As the results from the model development, it is found that different types of population require different sets of the utilities. Hence, there are 19 proposed IFD models based on types of populations and number of members in the household. Results from the model validation processes also presented that all 19 IFD models were successfully simulated the activities (ACT) and the decisions of whom in the household to do activities with (WHO).

The IFD model is expected to be better represent individual activity decisions than the Classification and Regression Tree (CART) model and the Bayesian network model as its incorporated the utility scores on the decision processes. However, practically, the performances of these models are not yet compared. In order to proceed to the conclusions, the comparisons of these modeling approaches should be provided, in the further research.

REFERENCES

[1] A. M. El-Zonkoly , "Optimal placement of multi-distributed generation units including different load models using particle swarm optimization," Swarm and Evolutionary Computation, In Press, Corrected Proof. http://doi.org/10.1016/j.swevo.2011.02.003

[2] C. D. Wickens and Hollands, J. G., "Engineering Psychology and Human Performance (3rd Edition)," Prentice Hall Inc., 2000.

[3] G. T. Pulido and C. A. C. Coello "A constraint-handling mechanism for particle swarm optimization," In Evolutionary Computation, 2004, vol. 2, pp. 1396-1403.

[4] N. Wongchavalidkul and M. Piantanakulchai, "The Integration of Classification Tree and Sequence Alignment Method for Exploring Groups of Population Based on Daily Time Use Data," Applied Soft Computing, 2015, vol. 34, pp. 106-119.

[5] S. Russell and P. Norvig, "Artificial Intelligence: A Modern Approach (2nd Edition)," Prentice Hall., 2003.

[6] U. B. Kjarulff and A. L. Madsen, "Bayesian Networks and Influence Diagrams: A Guide to Construction and Analysis," Springer., 2008.

ACKNOWLEDGEMENT

A part of this research was funding by the SIIT's graduate scholarship. The author is also would like to thank you Assoc. Prof. Dr. Mongkut Piantanakulch for his advising all over the topic.

Natachai W. is currently a lecturer in Cluster of Logistics and Rail Engineering at Engineering Faculty, Mahidol University, Thailand. He received M.Sc. in Civil Engineering (Transportation) Howard R. Hughes College of Engineering. School of Civil and Environmental Engineering and Construction. University of Nevada Las Vegas. He also received his Ph.D. in Engineering (Transportation) from Sirindhorn International Institute of Technology, Thammasat University

Neural Network Modeling for Predicting Electric Power Generation From Sea Waves

Pisit Phokharatkul[1*], Visarut Ahkuputra[2], Chom Kimpan[3*] and Ekkarit Maneenoi[2]

[1]Department of Electronics and Telecommunications Engineering, Faculty of Engineering, Kasem Bundit University, Bangkok, Thailand
[2]Tellvoice Technology Co., Ltd. Bangkok, Thailand
[3]Faculty of Engineering and Technology, Panyapiwat Institute of Management, Nonthaburi, Thailand
E-mail: pisit354@gmail.com*, chomkim@pim.ac.th*

***Abstract*—Thispaper presents a development of a prototype 1 kW electricpower generation system from sea waves in the gulf of Thailand. The system consists of electrical generator and buoy, and installed on a steel frame. This system is far from shore about 200 meters and sea level 3 meters deep. The purpose of this study is to investigate the relationship between electric power and wave height including the other parameters in the system. The neural networks are used to train the wave height and electric power and consequently the electric power from sea wave can be predicted. The predicted values from neural network models and polynomial regressionwill be compared. The predicted values from neural network are more accuracy in linking the inputs to the outputs in a non-linear manner. The prototype power units have been performed at the Sirindhorn international environment park to verify the ability of neural network models.**

***Index Teams*—sea waves, neural network modeling, electricpower generation, wave height**

I. Introduction

From the announce agreement, Kyoto protocol which sets a long-term goal of 50% reduction in global greenhouse emissions by 2050 is being negotiated [1, 2]. Thus, the importance of clean energy source for the next decades is interested. The potential of wave energy is tremendous and has led researchers to study in forecasting energy. They try to develop the wave farms commercially viable. However, temporal and spatial variability of wave height, frequency and direction is highly irregular, it is very difficult to design sea wave energy converter. Recently, researchers have been to try developed the power generation system from sea waves using the permanent magnet linear generators.

In this research, the main components consist of a floating buoy, linear generator and frame based. Normally, a location of installation is off-shore in deep-sea to obtain the high energy from the sea waves. Invice versa the cost of electric transmission and maintenance are increased because of long distance between wave farms and the land. To solve this problem, the researcher proposed the electrical generating farms at near shore. Each wave energy converter consists of a buoy with 1.2 meter diameter, 320 W permanent magnet generator from a washing machine and a gear box with a ratio of 7:1. Furthermore the system also requiresa measurement part.

The generators were tested to find the characteristics of them. The buoy and gear box were designed to maximize generation. Finally, the systems were constructed on the steel frame based at the Sirindhorn international environment park as shown in Fig. I. The generated electrical power, sea wave amplitude and displacement moving of buoy were recorded and created the model of electrical production from sea waves.

Fig. I. Electrical power generation system

II. Properties of waves

A. Linear wave theory

The condition of linear wave theory in two-dimension is used to solve the solution of velocity potential ϕ [3]. These conditions are the water is homogeneous and incompressible, the surface tension forces are negligible, and flow is irrotational, respectively. The velocity potential ϕ to satisfy the Laplace equation as follows:

$$\frac{\partial^2\varphi}{\partial x^2}+\frac{\partial^2\varphi}{\partial z^2}=0 \quad (1)$$

where x and z are the horizontal and vertical coordinates, respectively.

Under these conditions, the wave height is small compare wave length and water depth. The particle velocities are proportional to the wave height, and wave celerity which is related to the depth and wave length. The surface deformations at the air-sea boundary incur the surface wave and they are characterized by the wave length L, or the wavenumber $k = \frac{2\pi}{L}$. The waves are propagating with the height H at the height d over the sea floor. A two-dimension diagram of wave propagating in the x direction is shown in Fig. II In Fig. II, L is defined as the horizontal distance between two successive wave crests, which is related to the water depth d and the wave period T, or reciprocally to the angular frequency $\omega = \frac{2\pi}{T}$. The speed of waves defined as the distance L divided by the wave moves in time T, or mathematical term $C = \frac{L}{T}$. The instantaneous elevation of thewater surface heaveis explained by the function of position and time $\eta(x, t)$.

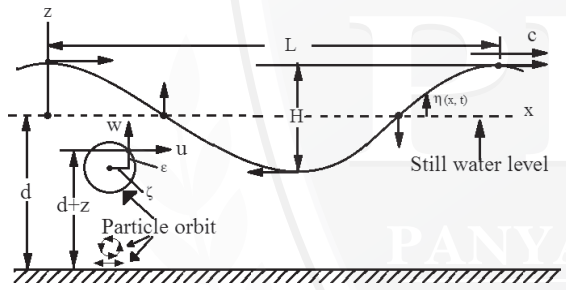

Fig. II. Definitions of linear water wave theory

Thus, the wave steepness defined as the ratio between the wave height and wavelength. The relative depth defined as the ratio between the water depth and wave length. The solution of equation (1) subject to the boundary conditions as:

$$\varphi = \frac{ga}{\sigma}\frac{\cosh k(y+d)}{\cosh kd}\sin(kx-\sigma t) \quad (2)$$

$$= \frac{gHT}{4\pi}\frac{\cosh[\left(\frac{2\pi}{L}\right)(y+d)]}{\cosh\frac{2\pi d}{L}}\sin 2\pi\left(\frac{x}{L}-\frac{t}{T}\right) \quad (3)$$

$$\eta(x,\,t) = \mathrm{a}\cos(kx-\sigma t) = \frac{H}{2}\cos 2\pi\left(\frac{x}{L}-\frac{t}{T}\right) \quad (4)$$

$$\sigma = (gk\tanh kd)^{\frac{1}{2}} \quad (5)$$

or $$C = \left(\frac{gL}{2\pi}\tanh\frac{2\pi d}{L}\right)^{\frac{1}{2}} \quad (6)$$

or $$L = \frac{gT^2}{2\pi}\tanh\frac{2\pi d}{L} \quad (7)$$

where x, z are Cartesian co-ordinates with z = 0 at the still water level (positiveupwards),

η(x, t) is the free water surface,

t is the time,

u, w, are the velocity components in the x, z directions,

ϕ or ϕ(x, y, t) is the two-dimensional velocity potential,

ρ is the fluid density,

g is the gravitational acceleration,

a is wave amplitude = $\frac{H}{2}$,

H is the wave height,

k is the wave number = $\frac{2\pi}{L}$,

L is the wave length,

f is the wave frequency = $\frac{2\pi}{T}$,

T is the wave period,

d is the mean water depth, and

C isthe wave celerity = $\frac{L}{T}$.

In deep water case: $\frac{d}{L} > 0.5$, $\tanh\frac{2\pi d}{L} \approx 1.0$.

The surface waves depend on the relative depth ($\frac{d}{L}$). The waves travelled from deep water offshore into shallow water near shore, the wave length will decreases. So that, the $\frac{d}{L}$ is used to classify into two cases:

- Deep water case, $\frac{d}{L} > 0.5$, $\tanh\frac{2\pi d}{L} \approx 1.0$

$$\therefore \quad L_0 = \frac{gT^2}{2\pi} = 1.56T^2 \quad (8)$$

- Shallow water case, $\frac{d}{L} < 0.04$, $\tanh\frac{2\pi d}{L} \approx \frac{2\pi d}{L}$

$$\therefore \quad L_0 = \frac{T(gd)^{\frac{1}{2}}}{2\pi} = \sqrt{gd} \quad (9)$$

B. Particle velocities

The horizontal and vertical component of water particle velocity can be computed from the derivative of Laplace equations:

$$u = \frac{\partial\varphi}{\partial x} \text{ and } w = \frac{\partial\varphi}{\partial z} \quad (10)$$

Substitute the velocity potential ϕ into the equation (10), the horizontal and vertical of flow are given:

$$u = \frac{\pi H}{T}\frac{\cosh\frac{2\pi(z+d)}{L}}{\sinh\frac{2\pi d}{L}}\cos 2\pi\left(\frac{x}{L}-\frac{t}{T}\right) \quad (11)$$

$$w = \frac{\pi H}{T}\frac{\sinh\frac{2\pi(z+d)}{L}}{\sinh\frac{2\pi d}{L}}\sin 2\pi\left(\frac{x}{L}-\frac{t}{T}\right) \quad (12)$$

The equation (11) and (12) can be reduced into the simplify form as follows:

$$u = \frac{\pi H}{T}\frac{\cosh\frac{2\pi z}{L_0}}{\sinh\frac{2\pi d}{L}}\cos 2\pi\left(\frac{x}{L}-\frac{t}{T}\right) \quad (13)$$

$$w = \frac{\pi H}{T}\frac{\sinh\frac{2\pi z}{L_0}}{\sinh\frac{2\pi d}{L}}\sin 2\pi\left(\frac{x}{L}-\frac{t}{T}\right) \quad (14)$$

C. Pressure

The pressure distribution in the vertical is given:

$$\frac{p}{\rho g} = \frac{\cosh 2\pi\frac{z+d}{L}}{\cosh\frac{2\pi d}{L}}\eta - z \quad (15)$$

D. Energy

The total energy per wave per unit width of crest E is:

$$E = \frac{\rho g H^2 L}{8} \quad (16)$$

The waves in water 100 m depth have a period of 10 s and a height of 2 m. These waves have a wave length of 156 m, wave celerity of 15.6 m/s, and the steepness is 0.013. While these waves propagated into a near shore depth of 2.3 m. The wave celerity is 4.15 m/s, wave length of 4.75 m, and the steepness is 0.048< 0.05.

III. The Energy Conversion Principle

A. Theory and data analysis

The total wave energy would be the sum of the kinetic and potential energy of buoy[4-6]. The electrical production system converted the wave energy to mechanical work, magnetic energy and electrical energy, respectively. Fig. III shows the block diagram of energy conversion. Sea wave is a sinusoidal waveform and time varying. The excitation inputs can be expressed as in equation (17).

$$D(t, x) = (A/2) \sin(\omega x + 2\pi x/\lambda) \quad (17)$$

where A is the amplitude of incident waves

ω is the angular frequency and

λ is the wave length.

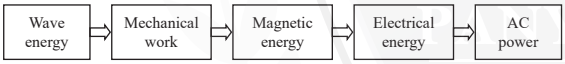

Fig. III. Block diagram of electrical power generation

The coupling configuration have the resultant ΣF is consisted of the hydrodynamic forces F_H, the gravitational force G, and the electromagnetism force F_G exerted via the system as follows:

$$\Sigma F = F_H - G - F_G \quad (18)$$

The hydrodynamic force depends on the movement of buoy and can be expressed as in equation (19).

$$F_w - G = \int_{-r}^{r} 2\sqrt{r^2 - x^2}\,[D(t,x) - S(t)]dx \quad (19)$$

where r is the radius of buoy, and

S(t) is the displacement of buoy.

The electromagnetism force exerted into the generator on the buoy always counter work its movement as follows:

$$F_G = NB^2l^2v \quad (20)$$

where N is the number of conductor in all slots,

B is the average magnetic field intensity of air gap,

l is the effective length of conductor and

v is the real time velocity of buoy.

From the equation (20) v depend on the wave height because of v = S/t. The velocity of buoy depended on the displacement of buoy but itindependent from a mass of buoy. However, the displacement of buoy related the amplitude of waves and mass of buoy. Thus, the design of buoy for maximizing converted the wave energy is very important [7, 8].

B. Development of artificial neural networks

The prediction problemin a case of electric power generation from sea waves is difficult because of the complexity of relationships in the input variables. Artificial neural network have been developed properly and typical parameters are employed to build the predicting electric power generation from sea waves. Similarly, the other power production such as the small hydropower plant [9], the prediction of electric power generation of solar cell [10], and the wind power plant [11], they have the same problems. From these problems, artificial neural networks offer an analyzing effectively to model performance of these plants, which have the complexity input variables.

This research applied the neural networks by approaching of feed-forward and back-propagation to compute performance predictions of electric power generation from sea waves. The power production depend on the characteristic of buoy, wave height, displacement moving of buoy, and the sea breeze in eachseason. Neural network as a functional estimator transforms inputs into outputs to the best of its ability as shown in Fig. IV The output of a neuron is a function in equation (21).

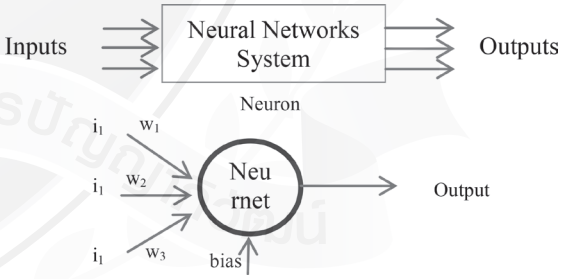

Fig. IV. Neural network as a function estimator transforms inputs into outputs

$$output = f(i_1w_1 + i_2w_2 + i_3w_3 + bias) \quad (21)$$

where i_1, i_2, i_3 are the inputs,

w_1, w_2, w_3 are the weighted in each inter-connection.

In next step, applied the output of each neuron to produce theoutput using sigmoid function $f(x) = \frac{1}{1+e^{-x}}$ where x is an input.The input of sigmoid functionis theoutput in equation (21) from each node. The weights of neural network are the most important factor of presenting network with some sample data and modifying the weights to better approximate the desired function. If the outputs are not correct,

the weights are adjusted according to the formula $w_{new}= w_{old}+\alpha$(desired-output)*input, where α is the learning rate. Train and adjust the network until the neural networks give the corrected output. Neural network in this research is used to predict the electric power production, especially in case of uncertainties of inputs and outputs operation.

C. The measurement of systems

In practical, the researchers recorded the AC power, the height of waves and displacement moving of buoy and consequently to build the model of electrical generating from these data. The height of waves and displacement of buoy were collected by a video camera. The system gets the color label data from the label tab as in Fig. V using the histogram methods. The number of pixels and the height of wave data were used to train the neural networks as the measurement model. After training, the measurement model is used to measure the height of waves and displacement of buoy automatically. The next step, the electric power, the height of waves and displacement of buoy data use to train the neural network as the prediction models. Since, the relation approximation between the AC power and the height of waves /displacement of buoy are cumbersome. The approximation depends on the amplitude of waves and the other parameter of system. This research proposes to find the available prediction model using neural networks as the detail in the next section.

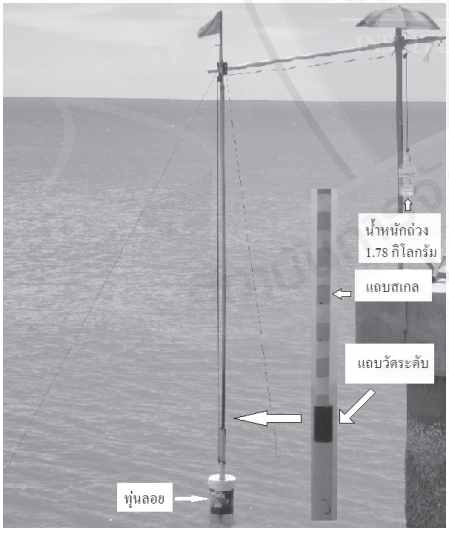

Fig. V. Label tab for measuring the height of waves

IV. Neural Networks as The Predicted Models

A complexity of mathematical model is used to predict the AC power from the height of waves and the other parameters. It is difficult to solve and find mathematical model [12]. However, the neural networks can be used to learn the knowledge of this relation as the predicted models. Thus, this research proposed to use the neural network as an approximation function. In Fig. VI, the unknown function is approximated using neural networks by adjust the parameters of the networks. So that it will produce the same response as the unknown function, if the same inputs are applied to both systems. In applications, the unknown function may correspond to a system as transform signals. Thus, the neural networks will be predicted the outputs from the inputs represent the mathematical model.

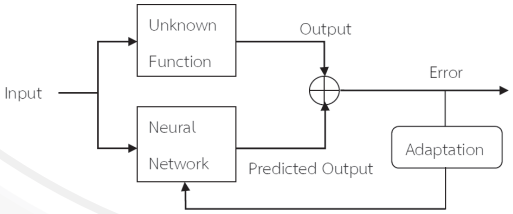

Fig. VI. Neural networks as an approximation function

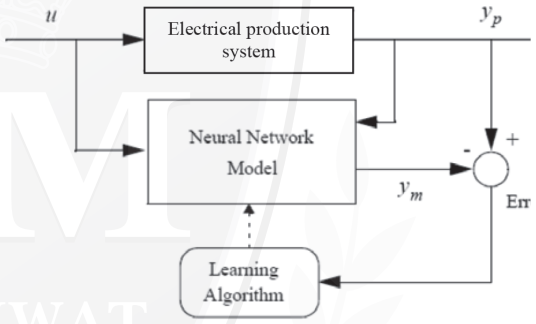

Fig. VII. Electrical production system identification

The first stage of prediction model is to train a neural network to represent the dynamic work of electric generator. Multilayer perceptron network with sigmoid transfer function is used to determine a procedure for selecting the weights and biases that will best approximation a given function. The selecting parameters or training uses back-propagation which is based on gradient descent. Fig. VII shows the electrical power generation system identification. From Fig. VII the difference errors between the electric generator outputs and the network calculated outputs are used as a neural network training signal. The error signals use to adjust the weights and biases of network for the special knowledge of this system. The weights and biases from the finish training is used as to predict the AC power output with related the wave height or displacement of buoy.

The next stage compares the calculated outputs from the predicted model with the calculated output from polynomial regression as the detail in section V.

V. The Experimental Results

In this study, the data testing is kept from the fieldwork at the Sirindhorn international environment

park in the gulf of Thailand. The wave height get from the label tab video images (Fig. VIII) and covert to numerical data using the measured model as the results in Fig. IX and Table I.

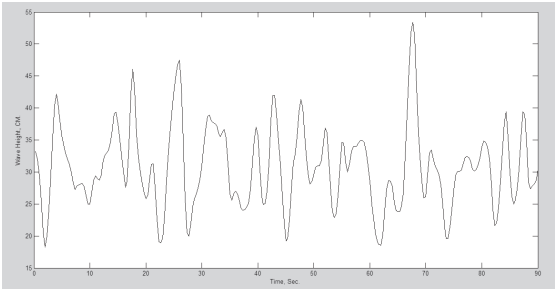

Fig. VIII. Graph of wave height

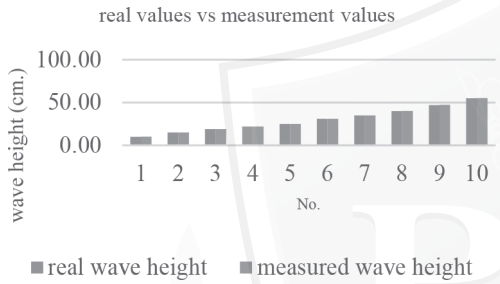

Fig. IX. Wave height from measurement model versus real wave height

TABLE I

Predicted valueswith real wave height

No.	real wave height (cm.)	wave height from the measurement model (cm.)	% |error|
1	10	10.24	2.40
2	15	15.14	0.93
3	19	18.98	0.11
4	22	22.02	0.09
5	25	25.03	0.12
6	31	30.95	0.16
7	35	35.00	0.00
8	40	40.20	0.50
9	47	47.30	0.64
10	55	55.22	0.40
	Average % |error|		0.54

The electric power outputs were recorded using watt meter and the wave elevations and displacements moving of buoy were recorded by the measurement model via the video camera. The wave elevation and electrical power output used as the order pair of inputs-outputs to adjust the weights and biases of networks. After training, the parameters of network used to build the predicted model. Fig. X and XI show the comparison results of the calculation results from the predicted models with the polynomial regression. Table II, IV shows the error calculations from predicted models with the Instantaneous electric powers.

TABLE II

Predicted values of predicted model and polynomial regression of unit 1

	Wave height (cm.)	Power measurement (W)	NN prediction (W)	% |error|	Polynomial Regression (W)	% |error|
1	20	20.78	20.78	0.00	20.70	0.39
2	30	22.17	22.17	0.00	22.26	0.42
3	40	28.20	28.68	1.69	28.80	2.12
4	50	45.90	45.99	0.20	43.88	4.40
5	60	64.01	63.84	0.27	66.30	3.57
6	70	91.45	91.67	0.24	90.02	1.56
7	80	104.20	103.47	0.70	104.25	0.05
			Average % |error|	0.44	Average % |error|	1.79

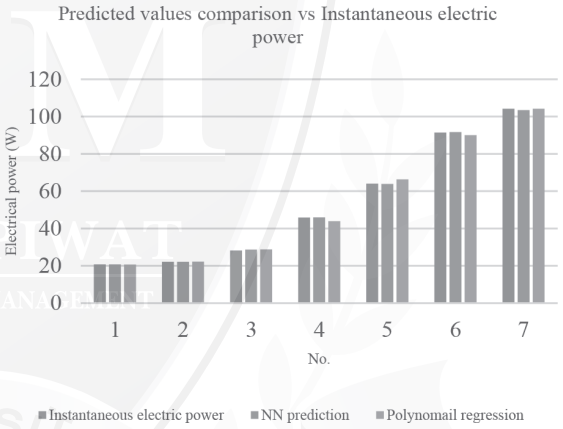

Fig. X. Predicted value comparison between the predicted model and polynomial regression

TABLE III

Instantaneous electric powers and predicted values (use wave height & displacement moving for training) of unit 1

	inputs		Instantaneous electric power (W)	Predicted electric power (W)	% | error|
	wave height (cm.)	displacement moving of buoy (cm.)			
1	20	9	20.78	20.78	0.00
2	30	14	22.17	22.17	0.00
3	40	18	28.20	28.20	0.00
4	50	23	45.90	45.90	0.00
5	60	27	64.01	64.01	0.00
6	70	32	91.45	95.81	4.77
7	80	36	104.20	104.20	0.00
Average % |error|					0.68

TABLE IV

PREDICTED VALUESOF PREDICTED MODELS AND POLYNOMIAL REGRESSION OF UNIT 2

	Wave height (cm.)	Instantaneous electric power (W)	NN prediction (W)	% |error|	Polynomial Regression (W)	% |error|
1	10	8.50	8.50	0.00	8.50	0.00
2	20	10.04	10.06	0.21	10.10	0.60
3	30	24.63	24.63	0.00	24.96	1.34
4	40	60.00	59.77	0.39	61.06	1.77
5	50	100.50	100.50	0.00	103.10	2.59
		Average % |error|		0.12	Average % |error|	1.26

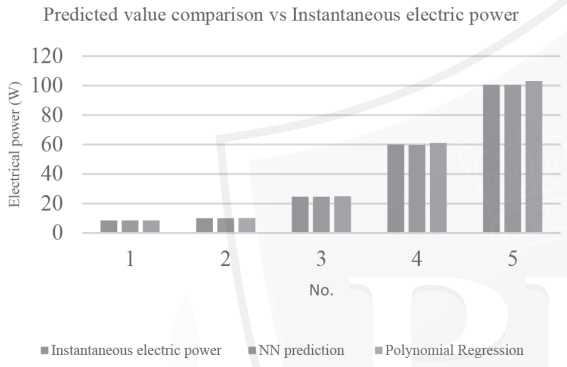

Fig. XI. Predicted values of predicted models and polynomial regression of unit 2

TABLE V

INSTANTANEOUS ELECTRIC POWERS AND PREDICTED VALUES (USE WAVE HEIGHT & DISPLACEMENT MOVING FOR TRAINING) OF UNIT 2

	inputs		Power measurement (W)	Power calculation (W)	% |error|
	wave height (cm.)	displacement moving of buoy (cm.)			
1	10	5	8.50	8.96	5.39
2	20	9	10.04	10.04	0.00
3	30	14	24.63	24.63	0.00
4	40	18	60.00	60.00	0.00
5	50	23	100.50	100.50	0.00
Average % |error|					1.08

VI. DISCUSSION AND CONCLUSION

The power outputs can be derived from equation (16) in Section II. We can to compute the power outputs using the different level of wave height data in Table II. For example at the wave height 30 cm. has the power output 110.25 W, while a measurement power output equals 22.7 W. Thus, the average efficiency of sea wave system of this research is about 19.25 %. The results of this research are corresponding with the result of research in [13, 14]. The model building takes data at least a year. The researchers study the uncertainties of parameter operation and design the network structure and trained by means of 340 experimental data. A generated electrical modeling from wave energy divided into parts: measurement model and predicted model. The two model performed calculation using neural network. In training stage, Neural networks try to adjust the parameters until satisfy with the knowledge and able to compute the output of models. Table I, it can be seen that the error of neural network model is 0.54%. Thus, this model can be used to measure the wave height. In the case, electrical power generation have the complex parameters. However, possible to train the neural networks as the predicted model from the inputs-outputs of systems. Table II and IV show the results of the predicted models using neural networks and polynomial regression compare with instantaneous electric powers of unit 1 and 2, respectively. The NN predicted models have the average error 0.44 % and 0.12 % which less than the best polynomial regression ($y = -0.2x^4 + 2.597x^3 - 8.098x^2 + 10.68x + 15.72$ in Table II and $y = -0.94x^4 + 11.03x^3 - 35.30x^2 + 44.84x - 11.1$ in Table IV). Table III and V show the average error from NN predicted models are 0.68 % and 1.08 %. The NN predicted models in Table III and V is trained using the two inputs (wave height and displacement of buoy) for computing the output of models. The results of these tables show the ability of neural networks as predicted models. From the testing results, the neural networks can to learn the knowledge of systems and use the networks as the approximation of models.

REFERENCES

[1] M. ozger, "Prediction of ocean wave energy from meteorological variables by fuzzy logic modeling.", *Expert Systems with Applications* 38, 2011, pp. 6269-6274.

[2] L. Rodrigues, "Wave power conversion systems for electrical energy production.", *RE&PQJ,* vol. 1, no. 6, March 2008, pp. 601-607.

[3] R. M. Sorensen, *Basic Coastal Engineering*, Second Edition, Springer Science+Business Media Dordrecht, 1997, pp. 9-30.

[4] S. phaiboon and P. Phokharatkul, "Sea Waves Power Generation by Using a Permanent Magnet Rotary Generator Drive: A Case Study in Gulf of Thailand.", *Advanced Materials Research* (Volumes 433-440), pp. 1126-1131.

[5] K. Rhinefrank, E. B. Agamloh, and A.Von Jouanne et al., "Novel ocean energy permanent magnet linear generator buoy.", *Renewable Energy*, vol. 31, pp. 1279-1298. 2006.

[6] N. M. Kimoulakis, A. G. Kladas, and J. A. Tegopoulos, "Power Generation Optimization From Sea Waves by Using a Permanent Magnet Linear Generator Drive.", *IEEE Trans. Magn*., vol. 44, pp. 1530-1533. 2008.

[7] P. Siddorn and R.T. Eatock, "Diffraction and independent radiation by an array of floatingcylinders.", *Ocean Eng*., vol. 35, pp. 1289-1303. 2008.

[8] O. Yilmaz and A. Incecik, "Analytical solutions of the diffraction problem of a group of truncated cylinders.", *Ocean Eng*., vol. 25, pp. 385-394. 1998.

[9] A. T. Hammid, M. H. B. Sulaiman, and A. N. Abdalla, "Prediction of small hydropower plant power production in Himreen Lake dam (HLD) using artificial neural network.", *Alexandria Engineering Journal*, 7 Jan. 2017.

[10] M. Kawaguchi, S. Ichikawa, M. Okuno, T. Jimbo, and N. Ishii, "Prediction of Electric Power Generation of Solar Cell Using the Neural Network.", *International Conference on Knowledge-Based and Intelligent Information and Engineering Systems KES 2006: Knowledge-Based Intelligent Information and Engineering Systems*, pp. 387-392.

[11] Z. Liu, W. Gao, Y. Wan, and E. Muljad, "Wind Power Plant Prediction by Using Neural Networks.", *2012 IEEE Energy Conversion Congress and Exposition (ECCE)*, pp.1-7.

[12] R. Zbikowski and K.j. Hunt, *Neural Adaptive Control Technology*, World Scientific, 1996.

[13] S. Phaiboon and K. Jailearnmee, "Fuzzy Electric Generation Modeling from Sea Wave Energy in Gulf of Thailand.", *International Conference of Electrical, Automation and Mechanical Engineering (EAME 2015)*, May 2015, pp. 441-443.

[14] S. Phaiboon and K. Jailearnmee, "Fuzzy model for predicting electric generation from sea wave energy in Thailand.", *2016 IEEE Region 10 Conference (TENCON)*, 22-25, Nov. 2016, Singapore, pp. 2646-2649.

Pisit Phokharatkul received the Doctor of Engineering (Electrical Engineering) from King Mongkut's Institute of Technology Ladkrabang, M. Eng. (Nuclear Technology) from Chulalongkorn University, M. Eng. (Electrical Engineering) from King Mongkut's Institute of Technology North Bangkok, B. Eng. (Electrical Engineering) from Patumwan Institute of Technology, and B.Ed. (Physics) from Srinakharinwirot University, Patumwan, Bangkok, Thailand, respectively. Currently, he is an Associate Professor at Department of Electronics and Telecommunications Engineering, Faculty of Engineering, KasemBundit University, Bangkok, Thailand. His research interests are in computational intelligence, wireless communication systems, and signal processing. He has published over 80 conference and journal papers.

Chom Kimpan received the Doctor of Engineering (Electrical Engineering) from King Mongkut's Institute of Technology Ladkrabang, M.Sc. in Electrical Engineering from Nihon University, Japan, and B. Eng. in Electrical Engineering from King Mongkut's Institute of Technology Ladkrabang, Bangkok, Thailand. Now he is an Associate Professor at Faculty of Engineering and Technology, Panyapiwat Institute of Management, Nonthaburi, Thailand. His research interests are in artificial intelligence, pattern recognition, and speech recognition. He has published over 100 conference and journal papers.

Visarut Ahkuputra received his D. Eng. in Electrical Engineering from Chulalongkorn University, Thailand. Now, he works with Tellvoice Technology Co., Ltd. His research topics are Speech Processing, Digital Signal Process, Social Media Management System.

Ekkarit Maneenoi received his Ph.D. in Electrical Engineering from Chulalongkorn University, Thailand. Now, he works with Tellvoice Technology Co., Ltd. His research topics are Speech Processing, Digital Signal Process, Social Media Management System.

PAPER FORMAT

Format

- Articles not more than 15 pages in length, single-sided A4 paper, margins (top, bottom, left, right) are 1 inch (2.54 cm)
- Abstract and References set to single columns, content is set to double column, first line indent 1 cm (0.39 inch)
- English font is **Times New Roman**, as follows:

Content	Font Size	Labeling
Title	24 (CT)	bold
Author	11 (CT)	bold
Author's affiliation amd E-mail	11 (CT)	regular
Content	10 (LRJ)	regular
Footnotes	8 (LJ)	regular
Table title (indicated above the table)	8 (CT)	regular
Table content	8 (LJ)	regular
Figure caption (indicated in the figure below)	8 (LJ)	regular
References Head	10 (CT)	regular
References	8 (LJ)	regular
Math and Equation : Please use either the Microsoft Equation Editor or the MathType add-on (http://www.mathtype.com) for equations in your paper		

CT = Centre Text, LJ = Left Justified, RJ = Right Justified, LRJ = Left & Right Justified

Composition of the article

1) Article title
2) Write (all) the author's name, and indicate the academic title (if any), position, work units and E-mail
3) Abstract; less than 250 words, 3-5 keywords
4) Content
   4.1) Academic articles, should have introduction, content and conclusion
   4.2) Research articles, should have introduction, literature review, research methods, results, discussion and summary
5) Reference
6) Pictures, tables, etc., must be used in numerical order in the article, provided the source correctly, cannot use other people's copyright.
   Chart should be colored contrastingly or in black and white. The original chart must submit separately.

Reference

1. **Cited in the main text**. Indicate the reference by name-year before or behind the cited content. For example, noted author, year of publication and page. Such as: Joe Smith (2014: 147) or (Newman & Cullen, 2007: 18-19) or (Joe Smith and team, 2014: 217-219)
2. **Cited after the article**. Put all bibliographicalreferences after articles, and order according to the author's name, please refer APA format. Such as:

Basic format for books:

[1] J. K. Author, "Title of chapter in the book," in *Title of His Published Book, x*th ed. City of Publisher, Country if not

[2] USA: Abbrev. of Publisher, year, ch. *x*, sec. *x*, pp. *xxx-xxx.*

Examples:

[3] G.O.Young,"Syntheticstructureofindustrial plastics," in *Plastics,* 2nd ed., vol. 3, J. Peters, Ed. New York: McGraw-Hill,1964,pp.15-64.

[4] W.-K. Chen, *Linear Networks and Systems.* Belmont, CA: Wadsworth, 1993, pp. 123-135.

Basic format for periodicals:

[5] J. K. Author, "Name of paper," *Abbrev. Title of Periodical*, vol. *x,* no. *x,* pp. *xxx-xxx,* Abbrev. Month, year.

Examples:

[6] J. U. Duncombe, "Infrared navigation—Part I: An assessment of feasibility," *IEEE Trans. Electron Devices*, vol. ED-11, no. 1, pp. 34–39, Jan. 1959.

[7] E. P. Wigner, "Theory of traveling-wave optical laser," *Phys. Rev*., vol. 134, pp. A635–A646, Dec. 1965.

[8] E. H. Miller, "A note on reflector arrays," *IEEE Trans. Antennas Propagat*., to be published.

Basic format for reports:

[9] J. K. Author, "Title of report," Abbrev. Name of Co., City of Co., Abbrev. State, Rep. *xxx*, year.

Examples:

[10] E. E. Reber, R. L. Michell, and C. J. Carter, "Oxygen absorption in the earth's atmosphere," Aerospace Corp., Los Angeles, CA, Tech. Rep. TR-0200 (4230-46)-3, Nov. 1988.

[11] J. H. Davis and J. R. Cogdell, "Calibration program for the 16-foot antenna," Elect. Eng. Res. Lab., Univ. Texas, Austin, Tech. Memo. NGL-006-69-3, Nov. 15, 1987.

Basic format for handbooks:

[12] *Name of Manual/Handbook*, *x* ed., Abbrev. Name of Co., City of Co., Abbrev. State, year, pp. *xxx-xxx.*

Examples:

[13] *Transmission Systems for Communications*, 3rd ed., Western Electric Co., Winston-Salem, NC, 1985, pp. 44-60.

[14] *Motorola Semiconductor Data Manual*, Motorola Semiconductor Products Inc., Phoenix, AZ, 1989.

Basic format for books (when available online):

[15] Author. (year,monthday). *Title.*(edition)[Typeof medium]. *volume (issue).* Available: site/path/file

Example:

[16] J. Jones. (1991, May 10). *Networks.*(2nd ed.)[Online]. Available:http://www.atm.com

Basic format for journals (when available online):

[17] Author. (year, month). Title. *Journal.*[Typeof medium]. *volume (issue),* pages. Available: site/path/file

Example:

[18] R. J. Vidmar. (1992, Aug.). On the use of atmospheric plasmasaselectromagneticreflectors. *IEEETrans. PlasmaSci.*[Online]. *21(3),* pp. 876-880. Available: http://www.halcyon.com/pub/journals/21ps03-vidmar

More detail information, Please read **Preparation of Papers for International Scientific Journal of Engineering and Technology (ISJET), http://isjet.pim.ac.th**

PIM
PANYAPIWAT
INSTITUTE OF MANAGEMENT
สถาบันการจัดการปัญญาภิวัฒน์

Panyapiwat Institute of Management (PIM)
85/1 Moo 2, Chaengwattana Rd,
Bangtalad, Pakkred, Nonthaburi, Thailand 11120
Tel: 0 2855 1560 Fax: 0 2855 0392
htpp://isjet.pim.ac.th
E-mail: isjet@pim.ac.th, suchindacha@pim.ac.th